Title: **Upper Plate Structure and Splay Faults near the Kodiak Islands**

Authors: Marlon D. Ramos[1], Lee M. Liberty[2], Peter J. Haeussler[3], Robert Humphreys[3]

[1]*Air Force Research Lab*

[2]*Boise State University, Department of Geosciences*

[3]*United States Geological Survey*

This work is a non-peer reviewed preprint submitted to EarthArXiv. It is currently under review at *Geosphere*, special issue: *Subduction Top to Bottom 2*.

Social Media Twitter: @MarlonDRamos1

Upper Plate Structure and Tsunamigenic Faults near the Kodiak Islands

Marlon D. Ramos[1]
Lee M. Liberty[2]
Peter J. Haeussler[3]
Robert Humphreys[3]

[1]*Air Force Research Lab*
[2]*Boise State University, Department of Geosciences*
[3]*United States Geological Survey*

Corresponding author:
Marlon D. Ramos
ramosmd@umich.edu
https://orcid.org/0000-0003-4449-8624
Air Force Research Laboratory
3550 Aberdeen Dr SE
Kirtland Air Force Base
Albuquerque, NM 87108

ABSTRACT

The Kodiak Islands lie near the southern terminus of the 1964 Great Alaska earthquake rupture area and within the Kodiak subduction zone segment. Both local and trans-Pacific tsunamis were generated during this devastating megathrust event, but the local tsunami source region and the causative faults are poorly understood. We provide an updated view of the tsunami and earthquake hazard for the Kodiak Islands region through tsunami modelling and geophysical data analysis. Through seismic and bathymetric data, we characterize a regionally extensive sea floor lineament related to the Kodiak shelf fault zone, with focused uplift along a 50-km long portion of the newly named Ugak fault as the most likely source of the local Kodiak Islands tsunami in 1964. We present evidence of Holocene motion along the Albatross Banks fault zone, but suggest that this fault did not produce a tsunami in 1964. We relate major structural boundaries to active forearc splay faults, where tectonic uplift is collocated with gravity lineations. Differences in interseismic locking, seismicity-rates, and potential field signatures argue for different stress conditions at depth near presumed segment boundaries. We find that the Kodiak segment boundaries have a clear geophysical expression and are linked to upper plate structure and splay faulting. The tsunamigenic fault hazard is higher for the Kodiak shelf fault zone when compared to the nearby Albatross Banks fault zone, suggesting short travel paths and little tsunami warning time for nearby communities.

INTRODUCTION

Nearly the entire ~4000 km long Alaska-Aleutian subduction zone has ruptured in tsunamigenic M>8 earthquakes during the last century (Plafker, 1969; Carver and Plafker, 2008; Ryan et al., 2011). Spatial and temporal distributions of these large earthquakes have given rise to the notion that the subduction zone is segmented (Nishenko and Jacob, 1990), with the presumption that different portions of the fault have unique earthquake cycles. The last rupture near the Kodiak Islands resulted from the M9.2 1964 Great Alaska Earthquake (GAE; Figure 1). This earthquake initiated from the slip patch, or asperity, affiliated with the Prince William Sound (PWS) segment, where uplift of up to 12 m was measured along the Patton Bay splay fault system (Plafker, 1969; Liberty et al., 2013). The slip extended through the Kenai segment (Suito and Freymueller, 2009), and terminated approximately 700 km to the southwest, beyond the Kodiak Islands (Johnson et al., 1996; Ichinose et al., 2007).

On the Kodiak Islands, local tsunami run-up was observed in 1964 (Kachadoorian and Plafker, 1967; Figure 2), but sea floor displacements were not identified. The paleoseismic record shows evidence for many M8+ Holocene megathrust earthquakes associated with the Kodiak and adjacent segments (Nishenko and Jacob, 1990; Hutchinson and Crowell, 2007; Carver and Plafker, 2008; Briggs et al., 2014; Shennan et al., 2014 and 2018), but the location, geometry and slip history of faults that splay from the megathrust is unknown. Given the robust paleoseismic evidence of large megathrust earthquakes, understanding this region's fault kinematics are important to seismic and tsunami hazard analysis and risk mitigation.

85

86 As most of the Gulf of Alaska forearc is submerged (Figure 1), paleoseismic studies have mostly
87 relied on land elevation changes and the coastal sediment record to extract regional subsidence
88 and uplift signals from earthquakes. However, these records do not uniquely constrain
89 earthquake sources, cumulative slip estimates, or along-strike rupture limits from past
90 earthquakes. Modern seismic, geodetic, and paleoseismic data suggest that M7+ earthquakes
91 occur near the Kodiak Islands region every few decades, tsunami-capable M8 earthquakes have
92 a median return-period of a hundred or more years, and multi-segment M9 great earthquakes
93 have even longer return periods (Shennan et al., 2014). This temporal mismatch in coseismic
94 behavior between the Kodiak segment and neighboring subduction zone segments suggest
95 differences in strain accumulation and release along the plate interface. These differences may
96 be preserved in upper plate structures. Geophysical data have the potential to map active faults
97 and to characterize along-strike variations in upper and lower plate structures that may
98 uncover millennial-scale seismic behaviors.

99

100 In this paper, we identify and characterize faults in the region of the Kodiak segment using
101 legacy and new bathymetric, seismic, and potential field datasets. We relate motion on these
102 faults to both the GAE and other post Last Glacial Maxima (LGM) Holocene earthquakes. We
103 use the distribution of mapped faults to characterize upper plate structure and to constrain the
104 asperity boundaries and potential earthquake rupture limits. We use bathymetry data to back
105 project first arrival tsunami travel times that were recorded during the 1964 earthquake and to

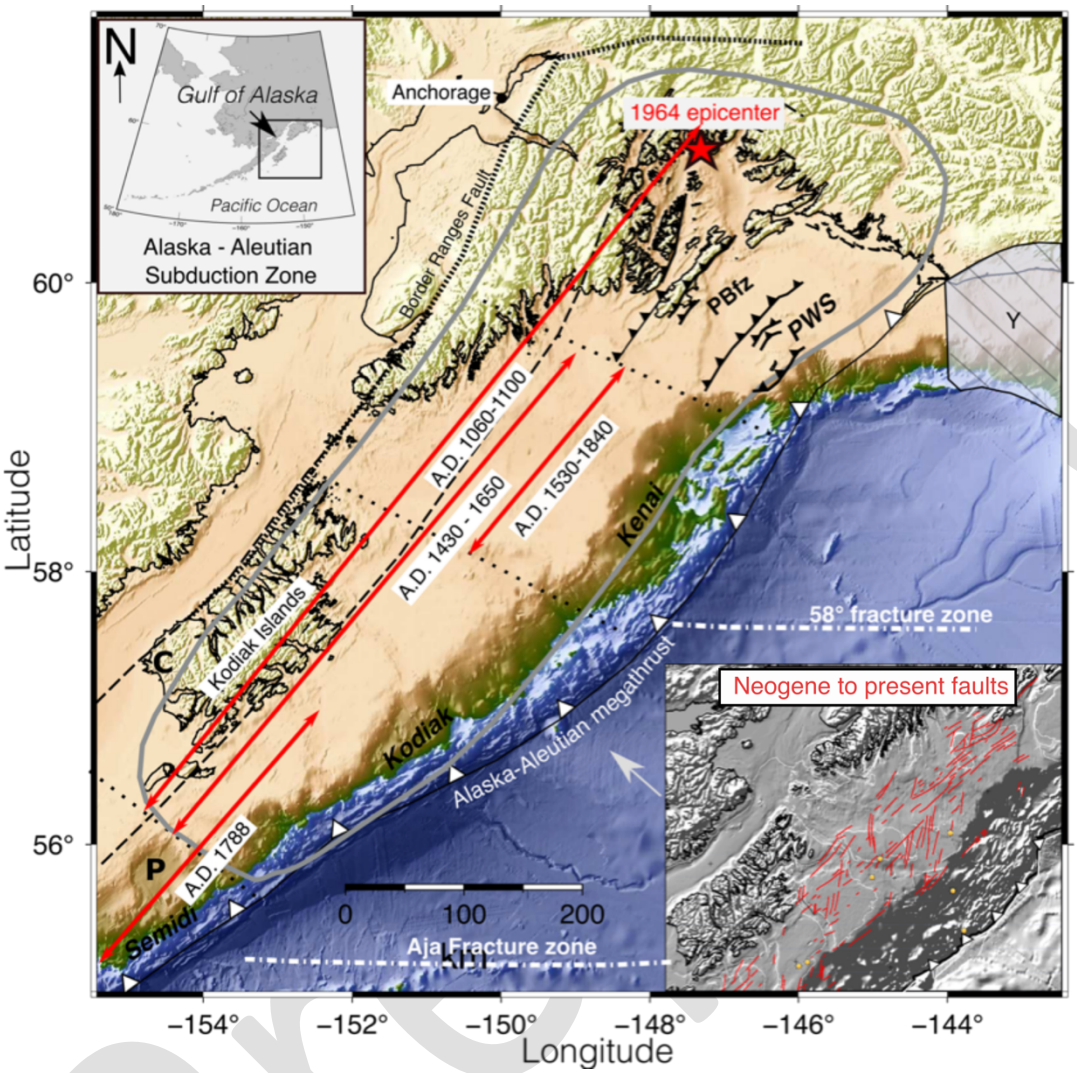

Figure 1. Great Alaska earthquake (GAE) rupture area (gray line) with shaded relief topography of the Gulf of Alaska region. Arrows denote rupture extent and age of previous megathrust earthquakes (e.g., Carver and Plafker, 2008; Briggs et al. 2014; Shennan et al., 2014). Patton Bay fault zone (PBfz) near Prince William Sound (Liberty et al., 2019) represents the region of maximum uplift during the GAE. Dotted black lines denote inferred subduction zone segment boundaries (Nishenko and Jacob, 1990; Suito and Freymueller, 2009). Inset map shows Neogene and active seafloor scarps interpreted as mostly reactivated reverse or thrust faults (red lines). Major fracture zone structures subducting below the Kodiak forearc include the Aja and 58° fracture zones. Top inset represents the greater Alaska-Aleutian subduction zone. P=Prince William Sound terrane, C=Chugach terrane, Y = Yakutat terrane. Colormap from Crameri (2018).

identify tectonic scarps. We identify the faults that lie beneath these scarps with seismic reflection data and estimate splay fault geometries and uplift rates from these data. Finally, we use satellite free-air gravity and EMAG2 magnetic anomaly datasets (Maus et al., 2009; Sandwell et al., 2014) to infer upper plate deformation and assess signatures of segmentation around the Kodiak Islands.

TECTONIC SETTING

Tsunamigenic splay faults have been imaged within the Gulf of Alaska forearc through seismic and bathymetric data (von Huene et al., 2012; Liberty et al., 2013, Li et al., 2015, Haeussler et al., 2015, Liberty et al., 2019). Similar fault geometries and seafloor uplift patterns presumably span the length of this subduction zone, but differences in plate geometry and subducting structure may give rise to differences in forearc structures and earthquake potential. From teleseismic receiver function and crustal-scale active source seismic data across the Gulf of Alaska, we know that faults splay from the subduction interface where this megathrust dips to the north between three to nine degrees (Moore et al., 1991; Eberhardt-Phillips et al., 2006; Liberty et al., 2013; Kim et al., 2014; Haeussler et al., 2015; Becel et al., 2017, Hayes et al., 2018).

The Kodiak shelf fault zone (KSfz) and Albatross Banks (ABfz) fault zone have been inferred to control upper plate fault motions near the Kodiak Islands (Fisher and von Huene, 1980; von Huene et al., 1980; Moore et al., 1991; Carver et al., 2008). Although no direct evidence has tied

the KSfz and ABfz to the megathrust, we can presume that they splay from this boundary because of their similarity to splay fault structures already imaged on nearby subduction zone segments (e.g., Moore et al., 1991; Liberty et al., 2013; Haeussler et al., 2015; Becel et al., 2017).

Carver et al. (2008) mapped the on-land portion of the KSfz, and they named the largest fault the Narrow Cape fault. They determined a recurrence interval for surface displacing events on the fault of 1-2 ka, or more than five times longer than the average maximum recurrence interval for M>8 earthquakes on the Kodiak segment (e.g., Shennan et al., 2018). This suggested other faults may activate during large megathrust earthquakes. The trenchward ABfz has been seismically imaged close to the continental shelf break and contains forearc basin-bound, reverse faults (Figure 1; Fisher, 1980; Fisher and von Huene, 1980). However, slip and fault distributions were poorly constrained due to a lack of modern seismic imagery; and there is no direct evidence that this fault system is active. In contrast, splay faults associated with the PWS and Semidi segments have been better characterized with more modern seismic and bathymetry surveys (e.g., Brocher et al., 1994; Liberty et al., 2013 and 2019; Finn et al., 2015; Haeussler et al., 2015; Li et al., 2015; Becel et al., 2017, Shillington et al., 2015). Here, we revisit legacy seismic data sets, and complement these older data with newly acquired seismic data to better constrain the tectonic history of the Kodiak segment.

KODIAK SHELF BATHYMETRY

For our tsunami source and fault mapping analysis, we utilize a regional bathymetry dataset to identify Kodiak shelf seafloor scarps (NOAA National Centers for Environmental Information, 2004). The Southern Alaska Coastal Relief model for most of the continental shelf was compiled at a resolution of 24 arc-seconds, or a 720 m grid interval. We compliment the regional bathymetry dataset with higher-resolution 8-arc second bathymetry data, and from a new compilation that covers the western Kodiak Islands region (Zimmerman et al., 2019). We recognize that much of the continental shelf region has not been surveyed within the past 50 years, thus limiting our analyses. Regardless, our compilation shows that sea floor scarps related to the KSfz extend for at least 200 km, from offshore Sitkinak Island northeast to at least the Chiniak trough (Figure 3). These scarps are upwards of 50 m tall, greatest in height near Sitkalidak Island.

Most of Alaska's continental shelf has water depths of 100 m or less, and has been shaped by LGM ice loads, post-glacial deposition, and Holocene tectonism. Sea levels were approximately 120 m below modern levels during the LGM (e.g., Peltier and Fairbanks, 2006) and ice covered much of the continental shelf (Kaufman and Manley, 2004; Kaufman et al., 2011). Radiocarbon dating at Narrow Cape indicates it was deglaciated approximately 13 – 13.5 kya (Figure 2, 3b; Carver et al., 2008), likely resetting seafloor surface prior to that time.

The shallow shelf areas typically contain little unconsolidated sediment that reflect modern deposition. In contrast, cross-shelf glacial troughs are often more than 50 m deeper than the nominal shelf depth and are traps for modern deposition (e.g., Carlson and Molnia, 1975; Liberty et al., 2013; 2019). These unconsolidated sediments typically lie above a prominent shallow unconformity that likely represents the hiatus in deposition during glaciation (e.g., Figure 4e). Because many sea floor lineaments cross pre-Pleistocene depositional fabric, we assume that these represent scarps from Holocene fault uplift (e.g., Liberty et al., 2013; 2019).

FIRST-ARRIVAL 1964 TSUNAMI SOURCE

The 1964 GAE generated tsunamis that inundated shorelines around the Pacific Ocean. Plafker (1969) inferred a tsunami source from the continuation of the Patton Bay fault to have caused the first waves that arrived on the Kodiak Islands (Figure 2 and Table 1). However, the offshore extension of the Patton Bay fault was not mapped at that time. Subsequently, Liberty et al., (2019) showed that Holocene activity along the Patton Bay fault system diminishes to the southwest of PWS as large scarps do not extend across the Kenai segment (Liberty, 2015; Figure 1). Suleimani and Freymueller (2020) evaluated the role of splay faults and horizontal displacements from several regional coseismic slip models from the GAE and found they both locally had significant contributions.

To identify coseismic uplift near the Kodiak Islands, we use modern bathymetry (Figure 3), seismic reflection data (Figure 4), and a compilation of GAE tsunami first arrival times (Table 1).

We use tsunami first motions (estimated to the nearest minute) observed at seven sites on the Kodiak Islands relative to the main shock origin time (Plafker, 1969). We treat each run-up location as a wave source and back-propagate this source using finite differences (Figure 2). To derive a velocity field, we grid multi-beam and single beam bathymetry data at one-kilometer spacing and then convert depth to tsunami wave speed in each cell. We use La Grange's velocity-depth relationship, $v = \sqrt{gd}$, where d is the depth in meters and g is gravitational acceleration (Lamb, 1932). Each source is then back-propagated using this velocity field according to its respective tabulated travel time. We then compile individual wave-fronts from the final model to identify which sources could have shared the same tsunamigenic source location. Note that our approach cannot constrain tsunami wave amplitude and does not consider later arrivals; thus, we do not model near-shore, non-linear effects on tsunami wave propagation or identify additional tsunamigenic sources associated with later tsunami arrivals. Finally, we compare convergent source locations to identified trench-parallel scarps observed with seafloor topographic data and faults identified with seismic profiling.

The reported first sense of motion for six of seven run-up locations was up, consistent with the Kodiak Islands being located landward of the hanging wall of the Alaska-Aleutian megathrust (Plafker, 1969; Table 1). The one exception was at the northernmost Kodiak City measurement site. Of the seven tsunami sites, five back-projected wave-fields (Kaguyak, Saltery Cove, Cape Chiniak, Kalsin Bay, and Kodiak City) converge about 15 km south of Sitkalidak Island (Figure 2).

222 Here, we find a conspicuous 50-m-high trench-parallel seafloor scarp that we associate with the
223 KSfz (Figure 3). Two observations, Kalsin Bay and Old Harbor sites, do not share overlapping
224 wave-fronts, and arrive too late to be sourced from this region.

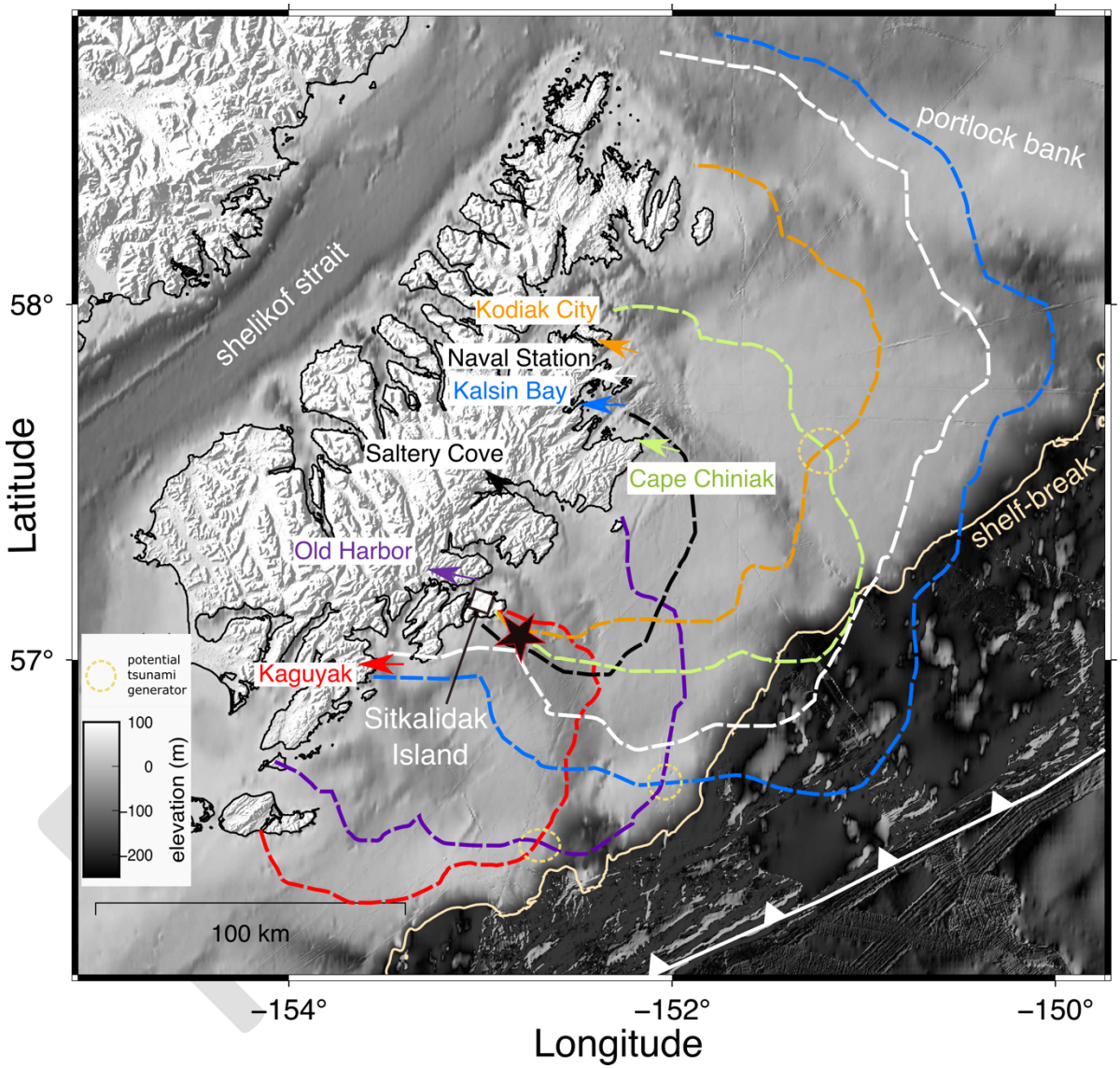

225

226 **Figure 2.** Results from tsunami travel-time modelling along seven run-up locations across the
227 Kodiak Islands. Back-propagated wave-fronts are colored according to run-up location and
228 represent the maximum distance a tsunami may have originated from based on the first
229 arriving wave crest. The star represents the estimated convergence region belonging to five

tsunami wave-fronts and our preferred tsunami source that is ~15 km south of Sitkalidak Island. We term this tsunami-generating fault the Ugak fault. SI=Sitkinak Island; S=Sitkalidak Island.

We note the reported first arrival time for Old Harbor is inconsistent with this interpretation; it is situated in a sheltered bay (Figure 2), and a direct tsunami wave from a fault located south of Sitkalidak Island may have experienced a more complex travel path. Thus, all but the measurement from Kalsin Bay is consistent with motion along the fault scarp near Sitkalidak Island (Figures 2 and 3).

Table 1. Tsunami travel times. Travel time difference in the third column is taken to be the relative difference in time between the source convergence point (-152.715 W, 57.061 N) and the closest distance to each modeled wave front. Modified from Plafker (1969).

Inundation Site	**Travel Time (minutes)**	**Travel Time Difference (minutes)**	**First Motion (reported)**
Kaguyak	38	6	NA
Old Harbor	48	24	Up
Cape Chiniak	38	0	Up
Kalsin Bay	70	13	NA
Naval Station	63	5	Up
Kodiak City	45	5	Down
Saltery Cove	30	0	NA

We infer only part of the KSFz moved in the 1964 earthquake. Had the faults near Kodiak City experienced significant uplift, tsunami wave crests would have arrived sooner to the north (Figure 2). Similarly, onshore KSfz fault segments did not show evidence for uplift in 1964. (Plafker, 1969; Carver et al., 2008). Thus, measurable uplift related to the GAE was likely limited to a narrow portion of the KSfz near the center of the Kodiak subduction zone segment.

While we infer uplift along a short segment of the KSfz during the GAE, KSfz seafloor lineaments have similar scarp heights along-strike (Figure 3). With scarp heights upwards of 50 m, and an estimated maximum coseismic uplift per event of about 8 m (Plafker, 1969), we conclude that 1) the region surrounding GAE uplift has repeatedly ruptured during Holocene megathrust earthquakes, 2) additional along-strike faults associated with the KSfz have ruptured in a similar fashion during past megathrust earthquakes, and 3) the entire length of this fault should be considered active and tsunamigenic.

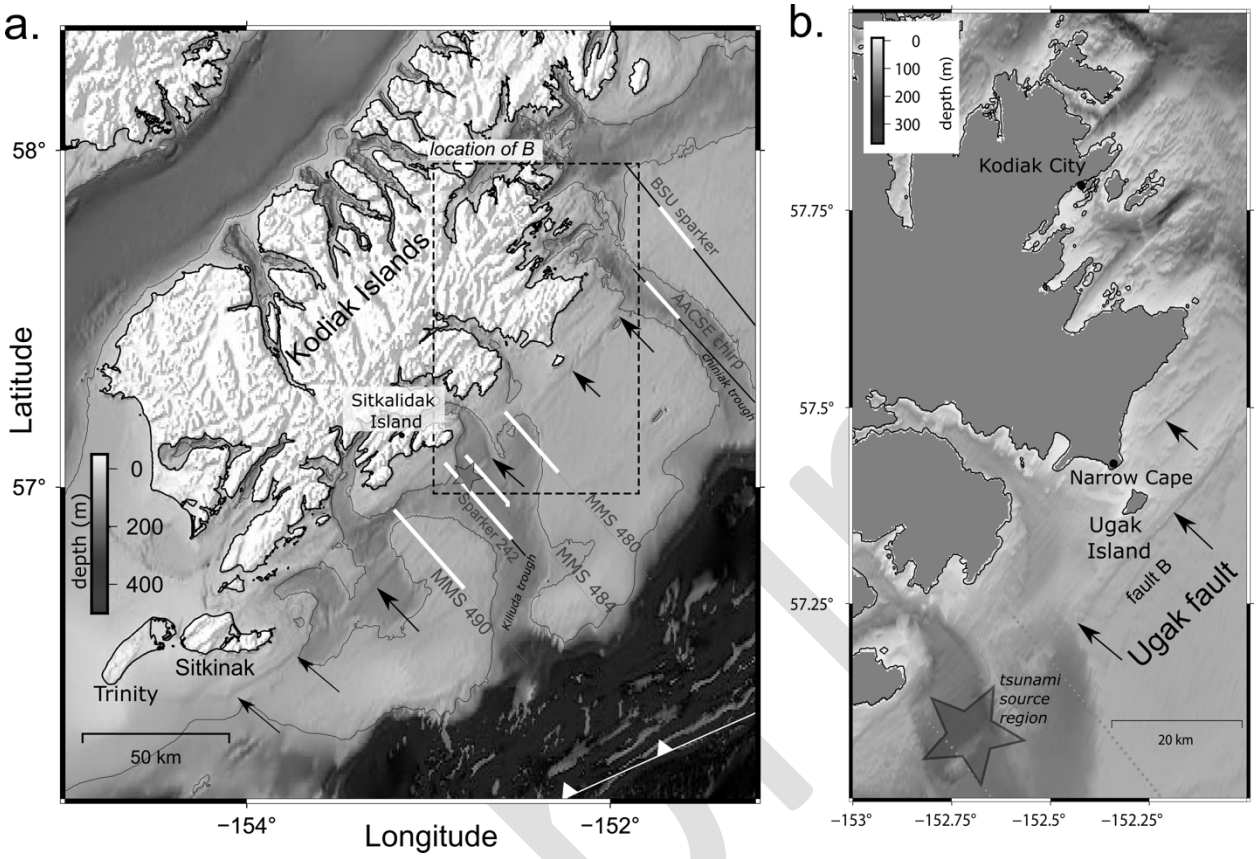

Figure 3. Kodiak Island Shelf zone and related faults. a) 24-arc second global bathymetry data with 100 m depth bathymetric contour. The map shows prominent NE-SW trending lineations belonging to the KSfz. Arrows identify prominent KSfz seafloor scarps. Labeled are seismic profiles (gray lines) and portions of the profiles presented in Figure 4 (white lines). B) 8 arc-sec bathymetry data in the dashed area of (a) showing ~20 m high Ugak and related faults highlighted with the seismic profiles. Gray region indicates region on land. Star represents our preferred 1964 tsunami source location.

While we show no direct evidence that the ABfz uplifted during the GAE, the convergence of three back-projected travel time contours from our tsunami analysis lies just beyond the edge of the continental shelf (Figure 2). Another notable convergence lies at an identified scarp along the ABfz (Figure 2; discussion below). Although we favor the KSfz tsunami source, our analysis

does not preclude co-rupture or later travel times from other sources. Indeed, assuming horizontal motion from the wedge slope, Suleimani and Freymueller (2020) identified the region near the continental shelf break as a likely tsunami source in 1964. Potential errors in the tabulated travel times (e.g., personal eyewitness accounts, timing) may point to inaccurate back-propagated locations for some of the observations. That said, while we see no compelling evidence for the GAE first arrival tsunami source along the ABfz, we will discuss a scarp and fault that is consistent with post-glacial Holocene uplift along the ABfz, closer to the Suleimani and Freymueller (2020) tsunami source region (see GAE tsunami source).

KODIAK SHELF FAULTS

To characterize Neogene and younger slip on the KSfz, we present a compilation of vintage and modern active-source seismic profiles that cross sea floor scarps (Figure 4). Given a 30 to 50 m up-to-the-north seafloor scarp near our tsunami travel-time convergence region (Figure 3), and that these KSfz-related scarps presumably developed over the past ~13.5 kya (Carver et al., 2008), we infer a long-term uplift rate of 2.2 to 3.7 mm/yr. If we assume (1) that the faults coseismically slip only during M>8 ruptures, and (2) that they have a recurrence interval of 400 years (i.e., 34 post-LGM earthquakes; Shennan et al., 2018), we would expect 1.4 to 2.3 m of uplift per M8+ earthquake along this fault. As our tsunami analysis suggests focused uplift in 1964, then the slip-per-earthquake and per-fault must be greater than the long-term average slip to produce multiple pronounced scarps related to the KSfz. Furthermore, the 8-m uplift

observed along the Patton Bay fault during the GAE (Plafker, 1969) suggests higher focused uplift is possible, and likely, to produce such fault scarps.

Seismic Reflection Profiling

Our seismic reflection dataset to characterize the KSfz consists of legacy 24-channel airgun seismic reflection profiles acquired in 1975 from the former Mineral Management Services of Alaska (MMS), a sparker seismic profile collected by the MMS in 1976, a chirp seismic profile acquired in 2018, and a sparker profile acquired in 2015 (Figure 4). The legacy seismic profiles were obtained as digital scans of stacked travel time images from MMS permit 75-02 (Liberty, 2013). The 2018 sub-bottom chirp data were provided to us from the Alaska Amphibious Community Seismic Experiment (Barcheck et al., 2020) and the 2015 sparker data were acquired using a 12-channel 500-Joule sparker seismic data on the US Geological Survey RV Alaskan Gyre (Liberty and Ramos, 2016). We migrate and depth convert the airgun images using stacking velocity values provided with the MMS image scans. We depth convert the chirp and sparker data using a velocity of 1,500 m/s. We interpret the seismic reflection data and show faults that offset the seafloor. We begin our analysis with profiles that cross our inferred 1964 tsunami source, then explore along strike profiles.

MMS line 484

311 Our back-projection model places the GAE tsunami source location along a northeast-trending
312 scarp close to MMS line 484 within the Kiliuda trough (Figure 3). Although this seismic profile is
313 low resolution (approximately 35 Hz center frequency or a 40 m predominant wavelength), we
314 note a 3.5-km-wide zone (CDP 145 – 180) where the seafloor is elevated about 50 m compared
315 to the surrounding regions (Figure 4). At CDP 140 and CDP 180, we note both truncated and
316 offset reflectors that increase in offset with depth, consistent with fault growth. We term the
317 fault at CDP 180 the Ugak fault, as this feature is located offshore of Ugak Island. Based on the
318 proximity to the convergence of tsunami travel time contours, we interpret coseismic uplift on
319 this fault as the first-arrival source for the 1964 tsunami that inundated several locations on the
320 Kodiak Islands. The seafloor lineation associated with this fault extends at least 80 km (Figure
321 3), suggesting that an independent rupture would be capable of generating a M7 earthquake
322 (e.g., Wells and Coppersmith, 1994). We interpret the fault that surfaces near CDP 140 (fault A)
323 as a south-dipping back thrust of the Ugak fault that controls the northern margin of the
324 upthrown block. It is also possible that fault A moved in 1964. The mottled seismic character
325 and rugged seafloor topography within the uplifted seafloor region (CDP 140 to CDP 180) is
326 consistent with deformed Cenozoic strata below the seafloor, similar to that mapped on the
327 Kodiak Islands (Moore et al., 1983). The parallel reflectors and smooth seafloor topography to
328 the south of the Ugak fault is consistent with late-Quaternary to Holocene marine strata. Here,
329 we interpret a strong-amplitude, seafloor-parallel reflector as the base of modern deposition.
330 Our interpretation is consistent with a regional unconformity that was seismically mapped
331 beneath PWS and the Gulf of Alaska, which likely defines the onset of post-glacial

sedimentation (i.e., Carlson and Molnia, 1975; Liberty et al., 2013; Finn et al., 2015; Haeussler et al., 2015; Liberty et al., 2019). We observe differentially offset reflectors across the Ugak fault and farther south, suggesting that additional faults near CDP 200 (fault B) and CDP 235 (fault C) have been Neogene-active (Figure 4d). Although poorly constrained, we estimate a fault dip of 70 to 80 degrees for the north-dipping faults. This dip is similar to the near surface expression of megathrust splay faults mapped near Montague Island (e.g., Plafker, 1969; Liberty et al., 2013; 2019). Using Hayes et al., (2018) slab 2.0 geometry and assuming simple planar or listric fault geometry, we project the Ugak fault to splay from the megathrust at ~30 km depth beneath the Kodiak Islands.

Faults B and C bound a 2-km-wide anticline that likely converge at about two to three km depth. The shallowest reflectors do not show measurable offset (upper 100 m below seafloor), suggesting that these faults may no longer be active, or measure low slip relative to sediment deposition rates. If the pattern of faulting observed on MMS 484 is characteristic of these fault zones, it may suggest that the majority of Holocene slip is focused on the more landward faults.

Sparker line 242

About 5 km to the southwest of MMS 484 and still within the Kiliuda trough (Figure 3), sparker seismic profile 242 shows the shallow character of the Ugak fault (Figure 4). In particular, this higher-resolution view (about a one meter dominant wavelength) of the Ugak fault shows a 25 m seafloor scarp near position 7 km. Here, we observe no modern deposition in the fault's

353 hanging wall to the northwest (hard water bottom, no subbottom reflectivity), an erosion
354 channel directly above the fault, and subparallel reflectors to the southeast of the fault that are
355 consistent with Holocene strata. We observe a second, more moderate seafloor high near
356 position 16 km that we interpret as the hanging wall of fault B. While we observe no
357 measurable seafloor offset on the MMS 484 across fault B, here we measure a seafloor offset of
358 about 5 m. Assuming these two features both represent fault B, we conclude that either this
359 fault is still active and the legacy airgun profiles do not provide adequate resolution to image
360 Holocene displacements, or the fault slip varies along strike. Although Fault C controls the south
361 limb of an anticline on MMS 484, this fault on Sparker 242 shows little evidence for Holocene
362 motion.
363
364 Assuming that the three identified faults along sparker profile 242 represent north-dipping
365 thrust faults, subbottom reflectivity suggests sediment deposition is focused on the seaward or
366 footwall side of each fault. At a deposition-rate of one mm/year (Carlson and
367 Molnia 1975), two notable subbottom reflectors at approximately 5 and 10 m below the
368 seafloor are consistent with early and mid-Holocene unconformities; the 10-m reflector
369 represents the Pleistocene-Holocene boundary. Similar age unconformities were inferred from
370 seismic profiles near the PWS region within the Gulf of Alaska (i.e., Liberty et al., 2013; Finn et
371 al., 2015), thus we suggest that these unconformities are pervasive, regionally significant, and
372 with detailed age controls, may be used to compare slip rates across subduction zone
373 segments.

374

375 *MMS line 490*

376 The northwest-southeast oriented MMS 490 is located 60 km to the southwest of MMS 484,
377 outside of the Kiliuda depositional trough (Figure 3). To explore the southwest extension of
378 active faulting, we trace sea floor scarps and examine the seismic character to identify the Ugak
379 fault at CDP 270, fault B near CDP 345, and fault C near CDP 370 (Figure 4). Here, based on
380 reflector offsets, we measure a fault dip of about 65° to the north for the Ugak fault and fault C,
381 and about 70° to the north for fault B. We observe that these faults show no measurable offset
382 of reflectors above about 100 m depth, suggesting little Holocene fault motion. Faults B and C
383 define the limbs of a four km wide fold with reflector offsets increasing with depth. Small
384 reflector offsets may indicate a back-thrust near CDP 200, but the convoluted reflection
385 polarities preclude rigorous interpretation of this portion of the profile. The change in dip angle
386 and reflector character on MMS 490 suggest reduced slip for the Ugak fault when compared to
387 MMS 484.

388

389 *MMS line 480*

390 Along MMS 480, located 20 km northeast of MMS 484, we identify the northeast extension of
391 the Ugak fault as a 30-m-high seafloor scarp with the bathymetry data (Figure 3). Near CDP 170,
392 we identify the Ugak fault from offset reflectors across a near vertical fault (Figure 4). As with
393 MMS 484 and MMS 490, we identify additional reflector offsets that we relate to faults A, B and
394 C. MMS 480 lies within the Kiliuda trough, suggesting comparable deposition and/or erosion

rates for MMS 484 and 480. We identify the greatest uplift of the Ugak fault closer to MMS 484. As with MMS 484 and MMS 490, MMS 480 shows a 4-km-wide anticline with no measurable sea floor offset. Here, this anticline is approximately twice the width when compared to MMS 484, consistent with oblique shortening away from the presumed tsunami source. This fault divergence was also observed near the focus of GAE uplift along the Patton Bay fault system (Liberty et al., 2019), suggesting that more detailed fault mapping is needed to improve our understanding of fault kinematics within the KSfz.

AACSE Chiniak Trough Chirp profile

Approximately 80 km to the northeast of the Kiliuda trough, we identify another cross glacial sediment trap termed the Chiniak Trough (Figure 3). Here, a 3.5 kHz Chirp reflection profile acquired on the RV Sikuliaq in 2018 captures a robust post-glacial sediment record. Along strike of the Ugak fault, we identify a 7.7 m sea floor scarp. Here, we measure a vertical offset of 18 m across a strong amplitude reflector that lies at the base of a package of subparallel reflectors that we presume are related to Holocene deposition (Figure 4). From the assumption of a 13.5 ka age basal marker, we estimate an average Holocene deposition rate of about 1.5 mm/year to the south of the Ugak fault, with a decrease in deposition rate to the north and south away from the fault. Assuming the offset on the interpreted post-LGM surface represents the Holocene slip rate, we estimate an uplift rate of about 1.3 mm/yr. This represents an uplift rate of about 25% of that observed along sparker profile 242 and MMS 484.

BSU Sparker profile

During 2016, we acquired a 500 J sparker seismic profile with a 12-channel hydrophone array across the northeast extension of the Ugak fault (Figure 3); termed BSU sparker profile (Liberty and Ramos, 2016). This profile lies about 20 km to the north of the Chiniak Trough sediment trap. Here, the latest bathymetric survey dates back to 1933, so it is unclear from sea floor data alone as to whether tectonic scarps are present. On the BSU sparker profile, our largest sea floor displacement that lies along-strike of the KSfz measures four meters. Across this scarp, we measure dipping reflectors in the upper tens of meters that are consistent with Quaternary fault motion. Although we identify no parallel reflectors that would point to Holocene deposition, we identify a reflection pattern that is consistent with some motion on the Ugak fault. With a diminished offset of the sea floor scarp compared to our seismic profiles to the southwest, we suggest that this profile shows where the KSfz becomes less active. We note that trench-perpendicular structures have been mapped to the northeast of this profile location, coincident with the presumed boundary between the Kodiak and Kenai segments (Figure 1; Fisher, 1980; Fisher and von Huene, 1980).

Summary of KSfz

From seismic and bathymetric data, we underscore two points. First, we note a divergence in distance between the Ugak fault and faults mapped to the south, consistent with oblique tectonic shortening along the KSfz. Second, the Ugak fault shows a maximum sea floor displacement along MMS 484 with diminished offset to the northeast and southwest. This may

437 suggest a repeated tsunami source near the Kiliuda Trough. While the Kiliuda Trough may be a
438 focus of exhumation, along strike sea floor scarps point to other tsunami sources that have
439 likely inundated the Kodiak Islands during past earthquakes.
440
441 Scarp heights measure higher on the seismic profiles when subparallel faults have separation
442 distances of 5 km or less (Figure 4). This might suggest that over a 20-30 km along-strike
443 distance, there are changes along the decollement that favor closer splay fault separation and
444 higher uplift rates. MMS 484 shows minor folding northwest of the Ugak fault, whereas
445 reflectors on MMS 490 are relatively undeformed and continuous. Between faults B and C,
446 however, reflectors suggest local shortening and growth faulting. These two faults merge at
447 depth, consistent with a more complex upper plate structure when compared to a model
448 where faults simply splay from the megathrust
449
450 Near Sitkinak Island (Figure 3), Zimmerman et al (2019) mapped two linear northwest-side-up
451 scarps that they relate to the KSfz. The northwestern of the two scarps is 20–25 m tall and 29
452 km long. The southeastern fault scarp, mapped only with single-beam bathymetry, may be
453 upwards of 45 m tall and 80 km long. These observations imply that although the Ugak fault
454 diminishes to the southwest, as mapped by MMS 490, the KSfz consists of many tsunamigenic
455 faults whose interactions are poorly understood or constrained. This pattern differs from that
456 observed along the offshore PWS faults, where a more focused exhumation region is observed
457 (Haeussler et al., 2015; Liberty et al., 2019).

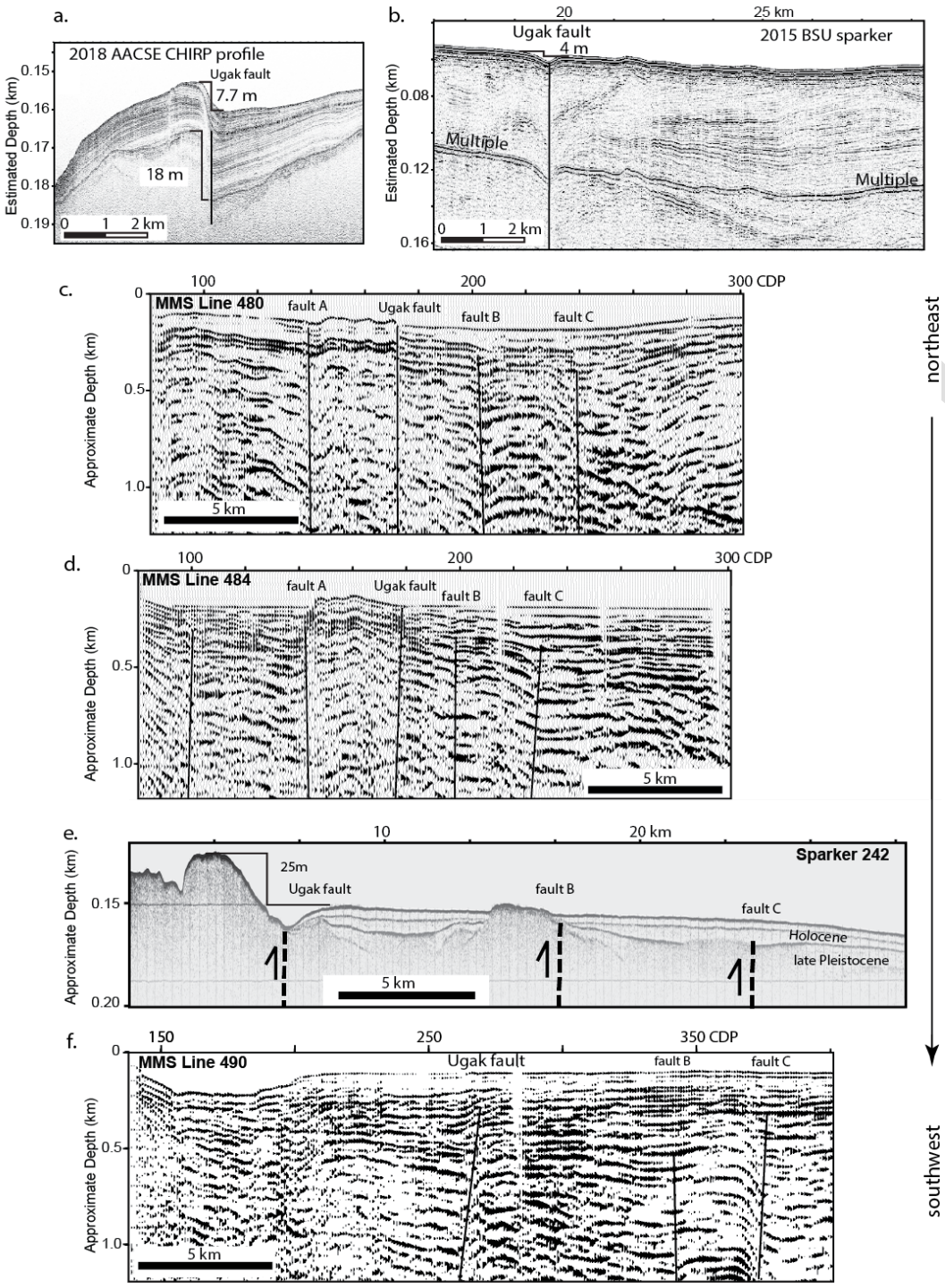

Figure 4. Chirp (a, b), MMS (c, d, f), and sparker (e) chirp seismic reflection profiles that cross the Ugak fault. Locations are noted on Figure 3. Profiles are oriented from northwest to southeast (left to right) and shown from northeast to southwest.

In summary, we find the ~200 km long KSfz contains variable scarp heights and along-strike variation in faulting style, although it is a long and laterally continuous structure. Large changes in seafloor scarp height and evidence for tsunami generation along the fault zone in 1964 argue for repeated, discrete KSfz uplift during megathrust slip, which translates to a high tsunamigenic fault hazard at distances close to populated areas. We presume that the KSfz splays from the megathrust near the southeastern limits of the Kodiak Islands. Coupled with onshore faults that indicate sinistral slip (e.g., Carver et al., 2008), the KSfz is a complex contractional fault system, which is possibly transpressional. Our observations warrant additional paleoseismic investigations. More detailed bathymetric and seismic mapping is needed to fully characterize the fault slip, interaction with the megathrust, and seismic hazard for this fault system.

ALBATROSS BANKS FAULT ZONE

The 250-km long, 40-50 km wide northeast-trending ABfz lies within the Kodiak forearc and contains a series of southeast-verging thrusts, reverse faults, and anticlinal structures that lie near the continental shelf edge (Fisher, 1980; Fisher and von Huene, 1980; von Huene et al., 1980; Figure 3). These faults bound a number of forearc basins, and each likely splay from the plate boundary at 20-30 km depth (Moore et al., 1991). While only single beam bathymetry data characterize the region surrounding the ABfz (NOAA National Centers for Environmental Information, 2004; Zimmerman et al., 2019), we present sparker and legacy airgun seismic profiles that constrain forearc structure and identify a possible tsunamigenic source.

From the low resolution 24 arc-second bathymetry dataset, we do not identify seafloor scarps near the shelf-break that are similar in magnitude and length to the KSfz (Figure 5). The few multi-beam tracks that pass through this area point to a single seafloor uplift that we explore here. Our initial bathymetric assessment, coupled with seismic results of Fisher (1980) and Fisher and von Huene (1980) is consistent with 1) a majority of Holocene fault motion, as observed on the seafloor, being accommodated around the KSfz and 2) that the currently available low-resolution bathymetry cannot capture the full seafloor expression of the ABfz. In other words, there are likely other sea floor scarps along the ABfz that we have yet to identify. These possibilities are examined in greater detail with seismic profiles.

GAE tsunami source

We begin our discussion of the ABfz in the vicinity of a prominent fault scarp that we identify on MMS 464 and the coincident BSU sparker seismic profile (Figure 5, 6). This location is consistent with tsunami travel times from Kodiak City and Cape Chiniak (Figure 2). Had this location solely sourced a tsunami, Plafker (1969) would have measured an earlier arrival time from the Kalsin Bay station and later arrival times from the other stations farther to the southwest (Table 1). Given two tsunami sources, one from the Ugak fault and one from this scarp, Plafker (1969) would have still observed an earlier travel time from the Kalsin Bay station (Figure 2). Thus, assuming accurate tsunami arrival times, we conclude that the fault that lies beneath this scarp did not produce tsunamigenic uplift during the GAE. It is possible that the shelf slope region

identified by Suleimani and Freymueller (2020) did produce a tsunami, but travel times from this location would have arrived later on all stations than what Plafker (1969) documented.

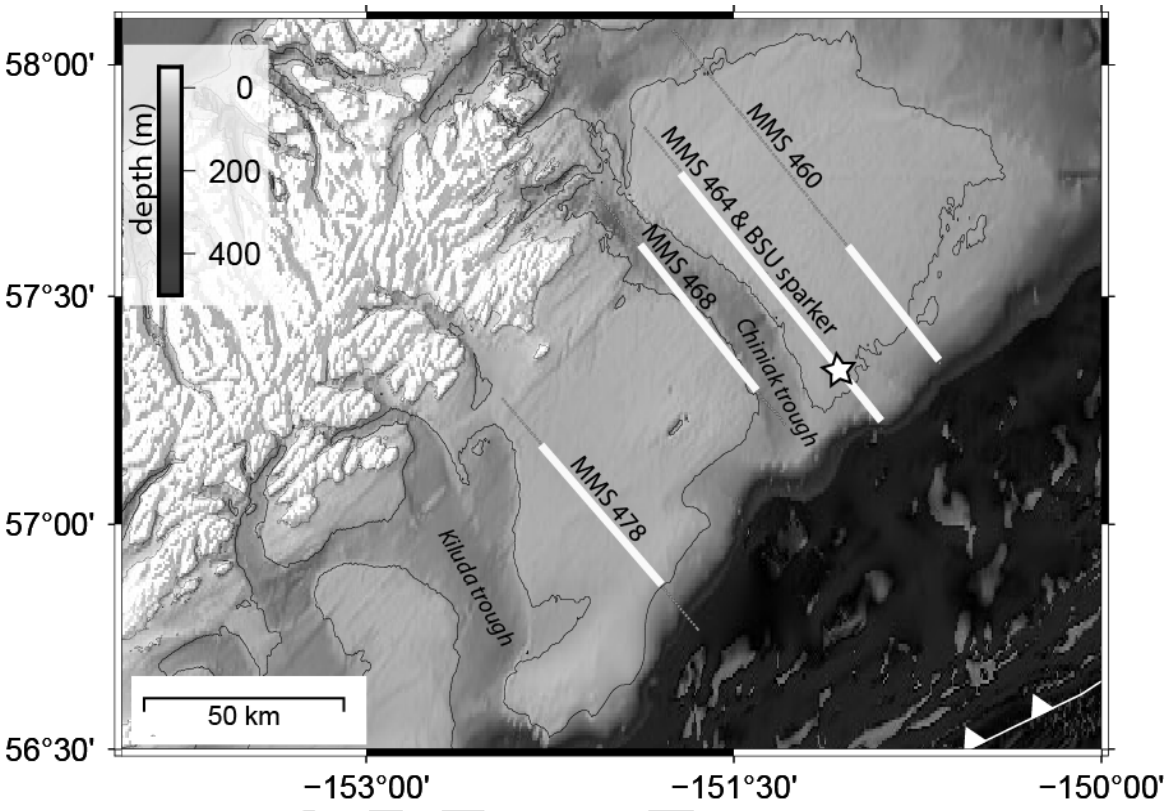

Figure 5. 24-arc second bathymetry across the Kodiak shelf detailing the Albatross Banks region and select MMS seismic profiles. Portions of the seismic profiles highlighted on Figure 6 are shown in white. The star represents a 16-m-tall scarp identified with MMS line 464 airgun and BSU sparker profiles. This is a possible tsunami source, consistent with Kodiak City and Cape Chiniak tsunami travel times.

MMS line 464 and BSU sparker profile

MMS 464 and the BSU sparker profile are coincident, lie immediately east of the Chiniak Trough, and both cross the KSfz and ABfz (Figure 5). Where these profiles cross the ABfz, we measure about a 16 m sea floor scarp (Figure 6). This scarp lies above a monocline that is

consistent with the upper plate expression of a megathrust splay fault (e.g., Liberty et al., 2013). We estimate a fault dip of about 80° on the shallow portion of this fault. The BSU sparker seismic profile shows south dipping strata and reflector truncations beneath the scarp. Given the seismic character and location on the shallow shelf, we interpret the shallow stratigraphy as representing pre-Holocene strata. Thus, a robust Holocene slip rate estimate was not possible for this fault at this location. However, with the assumption that seafloor topography was reset during the LGM, this fault has likely been active during many Holocene earthquakes. Thus, we interpret this scarp as tsunamigenic. If the 16 m scarp developed only over the past 13.5 ka, we estimate a slip rate of 1.2 mm/year.

MMS line 460

MMS 460 is located near the transition from the Kenai to Kodiak segment, 20 km to the northeast of MMS 464 (Figures 1 and 5). The seismic profile shows asymmetric, km-scale folding bound by three faults between CDP 640 and 725 (Figure 6). The distance between each ~70° SE dipping fault is less than 5 km and offset reflectors cannot be traced to the seafloor, implying relatively low Holocene slip rates. It is unclear how each of these faults relate to the presumed tsunamigenic fault highlighted on MMS 464, but the changing seismic character over a length scale of 20 km suggests that the ABfz is complex. The lack of a sea floor scarp suggests limited Holocene motion near the Kenai segment boundary.

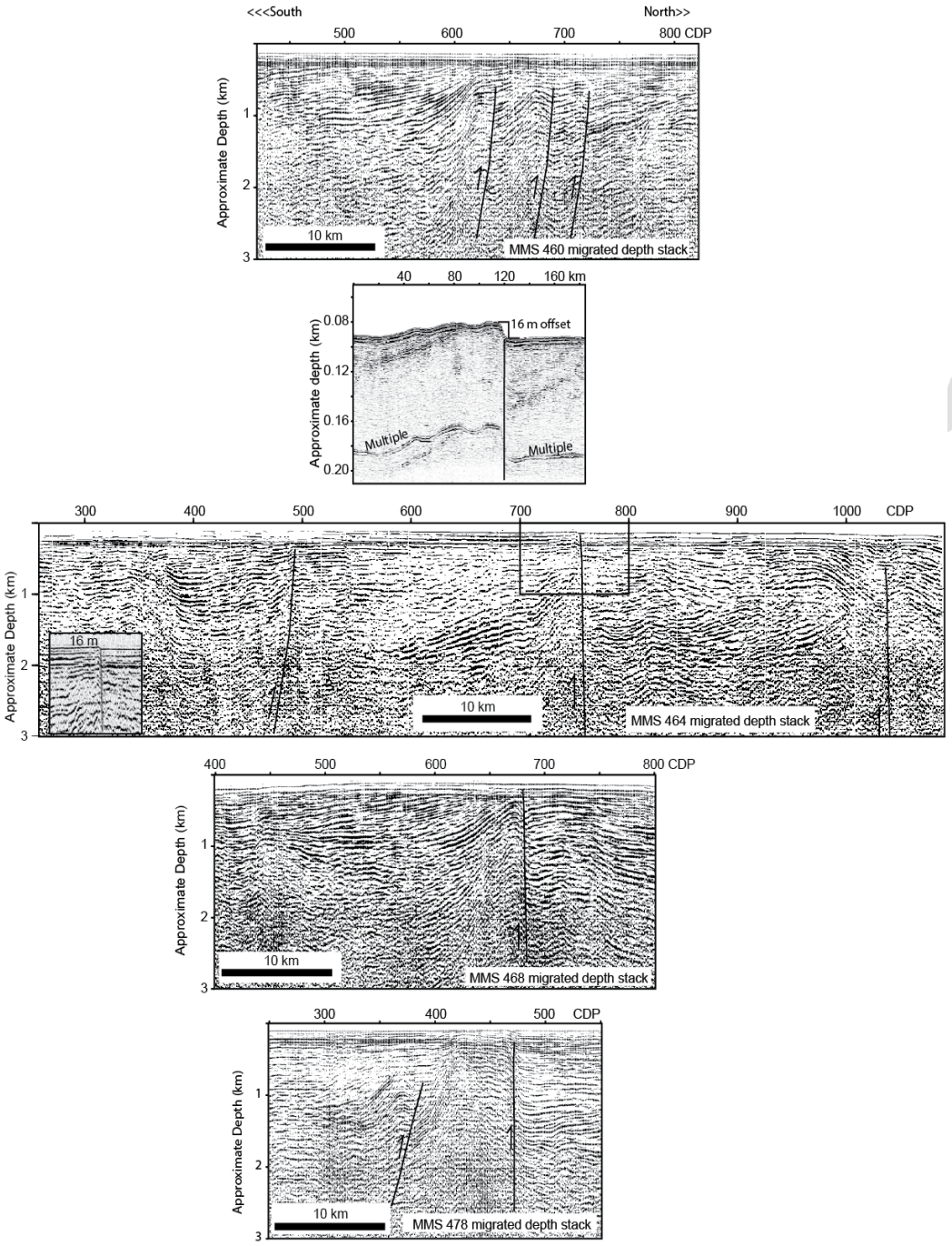

Figure 6. MMS airgun and sparker seismic reflection profiles of the Albatross Banks fault zone (ABfz). Sub-figures A, C, D and E show prominent splay faults that bound forearc basin structures, but do not appear to offset the seafloor. Sub-figure B, in contrast, shows a ~16-m high fault scarp that we imaged in 2015 with a sparker seismic source. We infer a Holocene slip-rate of 1.2 mm/yr for this particular fault.

544 *MMS line 468*

545 MMS profile 468, located 20 km to the southwest of MMS 464, crosses the Albatross Banks
546 near the Chiniak Trough (Figure 5). On this profile, we identify a single high-angle splay fault
547 near CDP 685 that lies along strike of the tsunamigenic fault identified on MMS 464 (Figure 6).
548 There is noticeable folding on the hanging-wall side of this presumed splay fault to less than
549 300 m below the sea floor. The fault does not appear to offset the sea floor. This suggests that
550 the tsunamigenic sea floor scarp is not regionally extensive and that focused uplift is restricted
551 to a narrow region surrounding MMS 464.

552

553 *MMS line 478*

554 MMS 478 lies between the Chiniak and Kiluda Troughs (Figure 5). We note a prominent
555 anticline centered near CDP 440 whose axis trends northwest-southeast (Fisher and von Huene,
556 1980; Figure 6). We identify two high-angle splay faults on this profile that are separated by
557 about 7 km. Folding is tighter across the northwest fault's hanging-wall (CDP 400) compared to
558 the hanging wall of the fault at CDP 460. We observe no shallow offset stratigraphy across
559 either fault, suggesting little to no Holocene motion.

560

561 ***Summary of ABfz***

562 Faults belonging to the ABfz are largely reverse faults originally mapped offshore Kodiak
563 between Sitkinak Island to the southwest and the Kenai segment boundary to the northeast
564 (von Huene et al., 1980; Figure 1 and 3). However, its near-surface architecture, Holocene

565 activity, and along-strike extent are largely unknown. Limited and generally low-resolution
566 bathymetry data for this region do not show conspicuous seafloor lineaments that we could
567 interpret as Holocene fault scarps (Figure 2 and 3). But the seismic data allowed us to identify a
568 16-m scarp that suggests recent tectonic activity. The MMS airgun seismic data do not have the
569 resolution to image seafloor offsets less than about 10 m, and this underscores the need to use
570 both high-resolution bathymetry and sparker seismic together to interpret fault activity.
571

572 **KSFZ AND ABFZ COMPARISON**

573 Although our datasets are limited, we find that both the scarp height and morphology
574 associated with the KSfz are much more prominent than those associated with the ABfz. Such
575 an observation implies a majority of Holocene faulting has been accommodated closer to the
576 Kodiak Islands shoreline (i.e., KSfz) rather than along faults nearer to the edge of the shelf (i.e.,
577 ABfz). This may indicate that through time, the location of focused deformation transitioned
578 from the outer to inner wedge regions of the forearc, which is expressed in the higher uplift-
579 rates of the KSfz compared to the ABfz we infer. One plausible hypothesis is that higher splay
580 fault activity (exhumation) is a function of the where the wedge changes from mechanically
581 weak (outer wedge) to strong (inner wedge backstop). In the PWS region, thermochronology
582 and seismic reflection data show that a major splay fault separates these regions (Haeussler et
583 al., 2015; Liberty et al., 2013). Rocks accreted before and after the subduction of a spreading
584 center in the Gulf of Alaska are similar in age between PWS and those onshore of the Kodiak
585 Islands (Bradley et al., 2003). This forms the strong-to-weak wedge transition and the location

of the KSfz roughly coincides with this structural boundary. Alternatively, the deformation rates have always been higher within the KSfz than the ABfz, which is still consistent with differences in wedge mechanical strength. We conclude that the tsunamigenic fault hazard is concentrated in the near-shore region of the Kodiak Island, although the ABfz and slope regions are still capable of producing tsunamis.

UPPER PLATE AND PLATE BOUNDARY STRUCTURE

Gravity and magnetic data can reveal unique signals of subducting and upper plate structure. While numerous studies have uncovered correlations between moment-release, subducting structure, and down-dip rupture limits (e.g., Wells et al., 2003; Song and Simons, 2003; Bassett and Watts, 2015), the Alaska subduction zone in particular seems to be more complex for understanding seismogenic behavior. A positive gravity anomaly dominates the Alaska forearc (Figure 7a) and this anomaly was interpreted by Wells et al. (2003) as resulting from a highly dense inner-wedge or duplexed structure near the plate interface. Seamounts and fracture zones on the Pacific plate offshore Kodiak are observed on gravity and magnetic data, but subducted expressions of these structures below the forearc are lacking (von Huene et al., 1999; Saltus et al., 1999; Mankhemthong et al., 2013; Figure 7a, b). Thus, the relationship between coseismic rupture, subducted topography, and upper plate splay faulting deserves further scrutiny for the Kodiak Islands region.

Gravity data

Free-air gravity anomalies over subduction zones map density differences related to either plate interface or upper plate structures (Smith and Sandwell, 1997). The spatial distribution of the free-air gravity field over the North American and Pacific plates near the Kodiak Islands shows several regional tectonic features that may influence seismogenesis (Wells et al., 2003; Bassett and Watts, 2015). We apply upward-continuation and bandpass filtering to the free-air gravity field to constrain the extent and geometry of the accretionary prism and upper-crustal faulting (Figures 7 and 8).

The free-air gravity map of the Kodiak-Kenai Peninsula region helps to clarify relationships between rock units in the accretionary prism. The Border Ranges fault zone marks the contact between the Mesozoic and Cenozoic accretionary prism and its backstop (Fisher, 1981; Plafker et al., 1994; Pavlis and Roeske, 2007; Mankhemthong et al., 2013). This fault coincides with a conspicuous gravity lineament that bounds the northwest extent of the Kodiak Islands (Figure 7a). To the southeast of the Kodiak Islands, a northwest to southeast transition from low to high gravity signals forms a lineation that defines the boundary between the older "Chugach terrane" part of the accretionary prism, and the younger Paleocene-Eocene "Prince William terrane" (Burns, 1985; Plafker et al., 1994; Wells et al., 2003). These two terranes are considered to divide the accretionary complex (Plafker et al., 1994), but the upper plate across this boundary consists of no discernable density contrast. Instead, this anomaly has been interpreted to stem from duplexing or other crustal densification processes near the plate

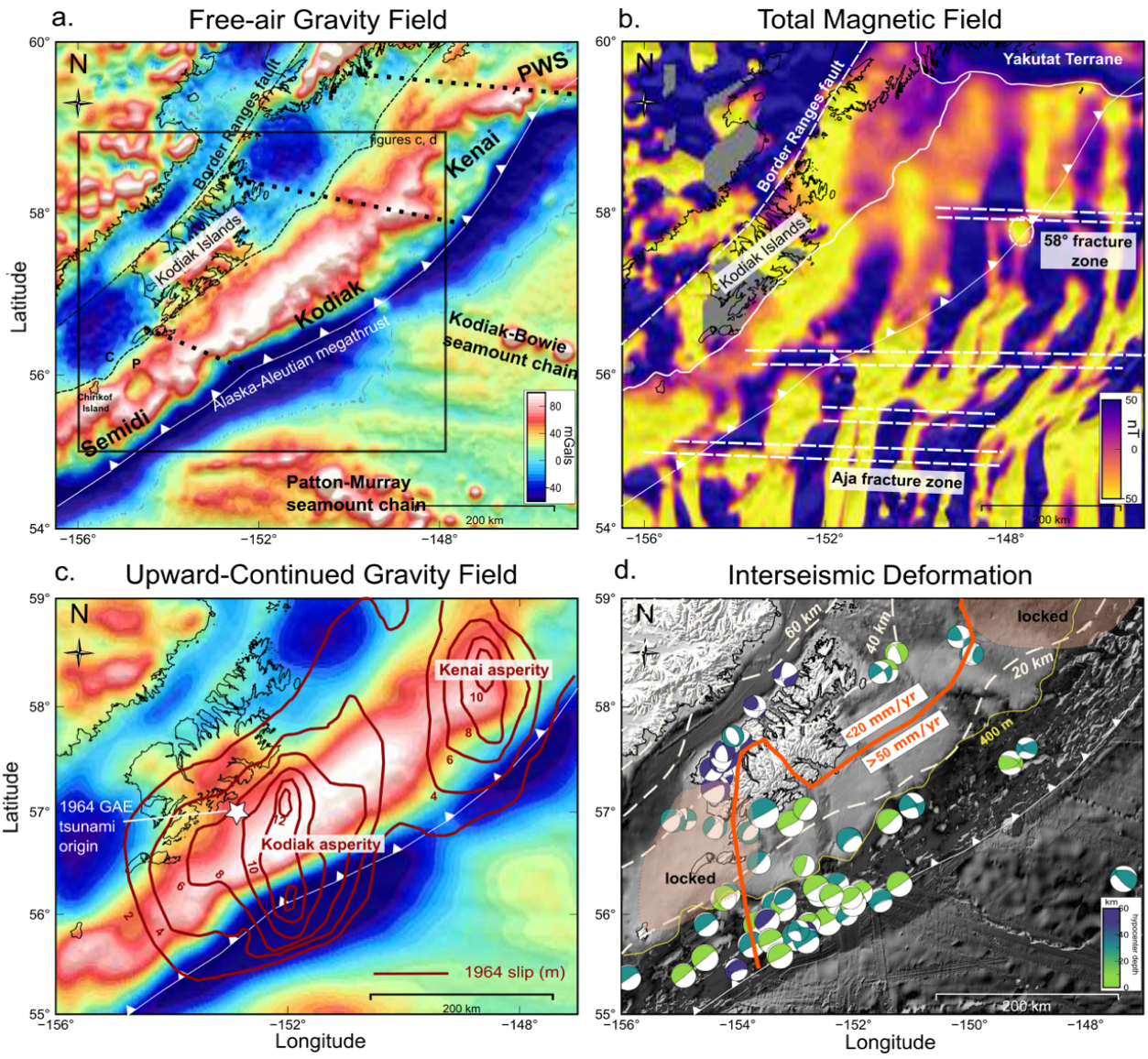

Figure 7. Geophysical expressions of crustal structure and segmentation across the western Gulf of Alaska. a) Free-air gravity anomaly map (Sandwell et al., 2014). Dotted black lines signify segment boundaries discussed in the text. Dashed black lines denote Border Ranges fault. Box denotes location of c and d. b) Total magnetic field from the EMAG2 database (Meyer et al., 2017). Gray regions represent data gaps. Solid white lines signify terrane boundaries. Major fracture zones (dashed white lines) from Naugler and Wageman (1973) are revealed as offset magnetic lineations. Note that several fracture zones (e.g., 58 °fracture zone, Aja fracture zone) appear landward of the trench. c) Upward-continued free-air gravity anomaly to a height of 10 km. Superposed are coseismic 1964 slip-contours (2 m) of Ichinose et al., (2007). We observe that slip was confined mostly to the positive gravity anomaly regions. d) Seafloor bathymetry map with post-1964 earthquakes (M > 5) colored by

hypocenter depth and plate locking model from Zweck et al., (2002). The 400 m bathymetry contour (yellow) delimits the continental shelf-break. The bold orange line signifies a major change in the slip-rate deficit as derived from geodetic inversion analysis (Li et a., 2016). Focal mechanisms from the CMT catalog (1976-2016) show the along-strike contrast in interseismic stress release following the GAE for the Kodiak region. Off-white dashed lines show the depth to the plate interface in 20 km intervals from the Slab2.0 model (Hayes et al., 2018).

boundary (Wells et al., 2003; Mankhemthong et al., 2013). In addition, significant rock uplift of the accretionary complex has brought higher velocity and presumably denser rocks closer to the surface. This regional exhumation process might also explain the source of the positive gravity anomaly (Ye et al., 1997) that may structurally link the KSfz and Patton Bay fault systems (Figure 7). Of note is that the related gravity lineation extends across segment boundaries where sea floor scarps and active faults have not been mapped.

We observe two circular gravity lows that bound the Kodiak Islands to the northeast and southwest, which were first noted by Wells et al. (2003) (Figure 7). These ~120 km wide low gravity regions lie between the Border Ranges fault zone to the north and the Prince William terrane boundary to the south. The limits of these gravity lows also coincide with our mapped extent of the KSfz (von Huene et al., 1980). The observed correlation between positive gravity anomalies and active splay faults suggests that offshore faults within the Prince William terrane (i.e., KSfz, ABfz) may have higher slip rates compared to faults closer to mainland Alaska.

Ye et al. (1997) identified a low seismic velocity mid-crustal body that spatially matches the large northern gravity low between the Kodiak Islands and Kenai Peninsula. This gravity/seismic

velocity low could be evidence for large-scale underplating of subducted sediment or a seamount as proposed by Ye et al (1997) and Mankhemthong et al (2013). The oblate negative gravity anomaly to the southwest of the Kodiak Islands does not correlate with any previously suggested upper plate (mid- to lower-crustal) source (Figure 7 and 8). The upper Miocene to Quaternary Tugidak basin has been mapped on Chirikof and part of the Trinity Islands, but this shallow basin may not account for the observed gravity low. Similar to the gravity anomaly that bounds the northeast side of the Kodiak Islands, we hypothesize that lower crustal underplating may be the source of this anomaly, as this feature persists even on the filtered long-wavelength component of the free-air gravity field (Figure 8).

Our examination of the gravity data does not further constrain this interpretation, however the spatial relationship between these two gravity lows that sandwich the high elevation Kodiak Islands may link underplated regions to lower exhumation rates. Moreover, the northeastern gravity low appears to correlate with our current understanding of subduction zone segmentation, and it correlates with a region of high slip-rate deficit outlined by Li et al. (2016) (Figures 7 and 8).

Farther southwest along the Semidi segment, the negative gravity anomaly becomes positive (Wells et al., 2003). This observation indicates a different crustal character between subduction zone segments. There exist few crustal seismic reflection data across this region (e.g., Becel et al., 2017). Robust forward potential field modeling of additional crustal-scale seismic reflection

684 data may be needed to assess underplating as a possible tectonic mechanism. If underplating is
685 occurring both northeast and southwest of the Kodiak Islands, this stresses the importance of
686 interface processes controlling splay fault activation and megathrust segmentation.
687
688 ***Magnetic data***
689 The total-magnetic field around the Kodiak Islands highlights several distinct tectonic structures
690 on the upper plate and topography on the incoming Pacific plate (Figure 7b). Some of these
691 continuous or offset magnetic lineations correspond to inferred earthquake segment
692 boundaries (von Huene et al., 1999; von Huene et al., 2012). In particular, the total magnetic
693 field shows offsets of the oceanic plate magnetic stripes that are most likely sourced by fracture
694 zones (Naugler and Wageman, 1973). The pattern of magnetic stripes is continuous across the
695 trench, showing that incoming plate structures are imaged below the accretionary wedge and
696 outer forearc (Figure 7b). Offset magnetic lineations on the incoming Pacific plate reveal at
697 least four main fracture zones that are presently subducting near, and beneath, the Kodiak
698 Islands. The Aja and two unnamed fracture zones are observed south of 57° N latitude. A
699 magnetic lineation related to the 58°N fracture zone persists almost to 200 km northwestward
700 of the trench, down to a plate interface depth of ~20 km (Hayes et al., 2018). This lineation lies
701 at the inferred northeast boundary of the Kodiak subduction zone segment (von Huene et al.,
702 1999; von Huene et al., 2012; Shennan et al., 2014). We note that although the KSfz lies
703 between the landward extension of the 58° N and Aja fracture zones, these features have

presumably migrated northwest with plate motions and there may be no relationship with the lateral extent of the KSFz (Figure 7).

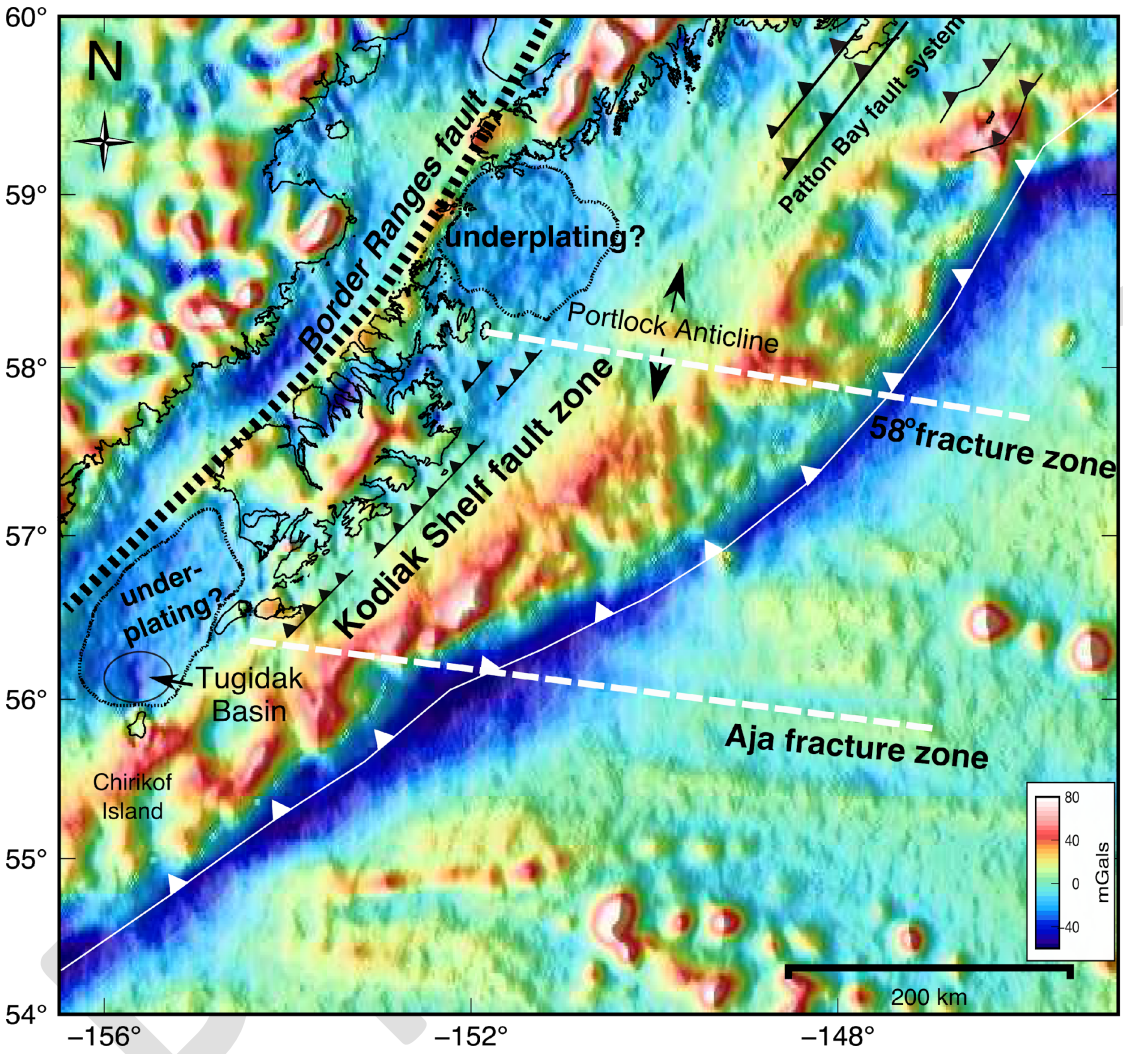

Figure 8. Low-pass filtered free-air gravity map for the Gulf of Alaska region. This map is filtered to remove signals with wavelengths greater than 100 km and shaded from the northwest to highlight gravity lineaments related to forearc splay faults and terrane boundaries. Note the continuity of the Kodiak Shelf fault zone and its gravity expression diminishes seaward of the Alaska forearc. Splay faults belonging to the Patton Bay fault system are also highlighted further to the north on the PWS segment. The gravity signature of the subducted 58° fracture zone within the wedge and its upper plate structural expression (Portlock Anticline) share the same N85W oblique trend. Two prominent low gravity anomalies south and north of the Kodiak Islands are interpreted as possible sites of

715 underplating. Note these two gravity lows bound both the mapped KSfz and the projection of
716 subducted 58° and Aja fracture zones (white dashed lines).
717

718 Both the Chugach and Prince William terrane boundary (seaward of the Kodiak Islands) are
719 revealed by magnetic field gradients, where the total-field switches from positive to negative
720 (Figure 7b). We consider magnetic anomalies to be features in the total magnetic field data that
721 disrupt the otherwise contiguous nature of upper plate magnetic signatures. A majority of both
722 the Chugach and Prince William terranes are characterized by negative total-field magnetic
723 anomalies, as expected of accreted sediments that contain little to no magnetically susceptible
724 minerals (Blakely, 1996; Saltus et al., 2007). Furthermore, this negative magnetic anomaly is
725 clearly bound by the Border Ranges fault system to the northwest; the northern region of the
726 magnetic domain of the Border Ranges fault has been referred to as the 'Knik Arm' anomaly
727 (Grants et al., 1963). In the northern Gulf of Alaska, the southern limit of the Yakutat terrane is
728 highlighted by a linear magnetic high anomaly that also coincides with the presumed
729 southwestern PWS segment boundary asperity (Bruns, 1983; Brocher et al., 1994). The major
730 magnetic domains evident on the upper plate are the Southern Alaska magnetic high and the
731 Chugach magnetic low which are sourced from dense lower crustal mafic and upper crustal
732 sedimentary rocks, respectively (Saltus et al., 2007).
733
734
735

736 **RELATIONSHIPS BETWEEN FAULTING, SUBDUCTING STRUCTURE, AND LOWER CRUSTAL DEFORMATION**

737 In order to relate structural controls of segmentation and subducting plate influences to upper
738 plate deformation across the Kodiak region, we compare 1964 earthquake slip models to
739 potential field and post-1964 seismicity and geodesy data (Figure 7c). Coseismic models from
740 the 1964 earthquake reveal three main slip-patches, or asperities, from joint inversions of
741 geodetic, seismic, and tsunami data (Johnson et al., 1996; Ichinose et al., 2007). The
742 southwestern, or Kodiak asperity, with 10 to 12 m slip, was focused below the shallow forearc
743 with down-dip rupture generally not extending across the Prince William terrane boundary
744 (Ichinose et al., 2007). The second asperity lies offshore the Kenai Peninsula and northeast of
745 the Kodiak Islands (von Huene et al., 1980; Ichinose et al., 2007). We refer to this ~100-km-wide
746 slip concentration as the Kenai asperity (Cohen and Freymueller, 2004; Kelsey et al., 2015).
747 When we upward continue the free-air gravity field to a height of 10 km, the resultant low-pass
748 gravity field shows that the high-slip regions of both the Kodiak and Kenai asperities are within
749 the positive gravity region (Figure 7c). We note that this particular slip inversion had limited
750 azimuthal seismic station coverage and inversion resolution is dependent upon three different
751 datasets (Ichinose et al., 2007). In general, forearc basin depocenters (negative gravity
752 anomalies) correlate with asperity location (e.g., Song and Simons, 2003; Wells et al., 2003),
753 however, here it does not, as previously noted for the Alaska-Aleutian subduction zone by Wells
754 et al. (2003) and Ichinose et al., (2007).
755
756 The 58° fracture zone divides the 1964 GAE slip maxima of the Kodiak and Kenai asperity
757 boundaries (Figure 7b, c). If this fracture zone is indeed a persistent segment boundary, the

758 1964 earthquake either had enough energy to rupture across the 58° fracture zone or perhaps
759 the fracture zone only halted rupture momentarily, as has been observed in another
760 megathrust earthquake (e.g., Robinson et al., 2006). Moreover, paleoseismic evidence indicates
761 the Kodiak asperity sometimes ruptures with, or sometimes independently of, the Prince
762 William Sound asperity (Shennan et al., 2014). Geodetic models show spatial distributions of
763 interseismic locking are different from coseismic strain release (Zweck et al., 2002; Suito and
764 Freymueller, 2008; Li et al., 2016). The 58° fracture zone does not show a strong gravity signal
765 on the incoming Pacific plate, which is likely due to 2 - 3 km of low-density sediment subducting
766 beneath the trench (Reece et al., 2011; von Huene et al., 2012; Gulick et al., 2015; Figure 7a).
767 The E-W magnetic lineament traces the 58° fracture zone beneath the Pacific plate and an
768 oblique N85°W trending (filtered) gravity anomaly coincides with this feature beneath the
769 wedge (Figure 8). The gravity field records differences in density due to structural juxtapositions
770 in upper plate deformation, which is probably driven by oblique convergence of the subducting
771 Pacific plate. Fracture zone morphology is typified by a large ridge and trough structure that
772 remains structurally competent as it spreads from the mid-ocean ridge and into the subduction
773 zone (Menard and Atwater, 1969; Sandwell, 1984). The outer wedge of subduction zones is the
774 mechanically weaker portion of the subduction zone forearc (Wang and Hu, 2006; Noda, 2016).
775 Wedges thus record recent and current deformation of subducting high-relief from the
776 incoming plate, such as seamounts or fracture zones (Basset et al., 2015). Considering both
777 fracture zone morphology and constraints from both potential field datasets, we interpret the
778 N85°W trending feature to be the upper plate expression of the subducted 58° fracture zone

779 below the outer wedge. Furthermore, a concentric anomaly in the total magnetic-field near the
780 trench suggests a subducted seamount may be associated with the 58° fracture zone (Figure
781 7b; Fruehn et al., 1999; von Huene et al., 2012).
782
783 The Kodiak segment transitions from strongly to moderately locked below the Trinity Islands
784 and northeast Kodiak Island (Figure 7d). This is in contrast to that observed with the PWS
785 segment, which is completely locked (Zweck et al., 2002; Sauber et al., 2006; Freymueller et al.,
786 2008). The gravity boundary between the Tugidak basin low and the higher values of Kodiak
787 Island correlate with geophysical expressions of this rupture boundary (Figure 7a). Moreover,
788 lower plate conditions change along the Gulf Alaska from PWS to the Kodiak Islands. For
789 instance, the trailing edge of the Yakutat terrane (Figure 7b) is highly coupled to the Pacific
790 plate. These structures together have much shallower dip (~4°) when compared to the Kodiak
791 region, where the dip gradually steepens to ~10° (Brocher et al., 1994; Eberhart-Phillips et al.,
792 2006; Sauber et al., 2006; Hayes et al., 2018). Roughness of the subducting Pacific plate could
793 also influence regional variations in coupling since there are numerous seamounts and fracture
794 zones sitting offshore from the Kodiak Islands, as shown in the potential fields data.
795
796 Post-1964 seismicity varies along-strike across the Kodiak Islands (Figure 7d). There is a relative
797 paucity of large earthquakes (M>5) for the northeast region and a majority of the seismicity is
798 occurring offshore and southwest of the Kodiak Islands, suggested by others to have occurred
799 in the subducting Pacific plate (Doser et al, 2002; Doser, 2005). Focal mechanisms in the

southwest Kodiak region are consistent with thrust faulting where the hypocenters cluster between 20 to 40 km depth. Models suggest the megathrust is mostly locked landward of these moderate seismic events (Zweck et al., 2002). However, shallow thrust events coupled with significant margin erosion, which may cause a shallowing of the slope angle, suggests that the southwest region of Kodiak may be in the underthrusting phase of the accretionary cycle (Gutscher et al., 1998). Underthrusting focused beneath the shelf may be accommodating some interseismic slip and may provide a means to maintain down-dip locking below southwest Kodiak. A lack of underthrusting near the plate interface may also explain why the KSfz tapers out across the Semidi segment (i.e. no exhumation mechanism).

Semidi/Kodiak segment boundary

Rupture models for a 1788 A.D., a 1440-1620 A.D., and a 1060-1110 A.D. earthquake recognize a semi-persistent boundary near the Trinity Islands (Briggs et al., 2014; Shennan et al., 2014; Kelsey et al., 2015; Figure 3). The oblique subduction of fracture zones and seamount chains could complicate megathrust interface conditions, upper plate deformation, and could exert enough structural control to act as a segment boundary (von Huene et al., 2012). There is a pronounced gravity gradient that parallels the KSfz. This lineament extends southwest of Chirokof Island and northeast to the Portlock anticline (Figures 7 and 8). While the gravity signature related to the KSfz terminates near the northern segment boundary, a similar gravity signature does not define the Kodiak/Semidi segment transition. The related lineation may

820 instead mark the location of the eroding continental shelf-break or alternatively, could
821 represent older splay faults that do not offset the seafloor.
822
823 Observations from multi-channel seismic reflection data (ALEUT experiment) across the Semidi
824 and Shumagin segments suggest that the hydration state of the megathrust and structure of
825 the incoming plate play pivotal roles in regulating seismicity and fault formation (i.e., Li et al.,
826 2015; Shillington et al., 2015; Li et al., 2018). Intermediate-depth earthquakes are more
827 abundant across the Shumagin and Kodiak regions, suggesting the Semidi segment is in a
828 different stage of the earthquake cycle (Shillington et al., 2015). In addition, these earthquakes
829 may be below the continental Moho, but ray coverage is insufficient to image deeper
830 megathrust structure in detail (Becel et al., 2017). Regarding upper plate structure, the central
831 Semidi segment appears to have several high-angle splay faults within the outer wedge,
832 seaward of the continental shelf break (Li et al., 2018). However, splay faults landward of the
833 continental shelf-break are largely unknown on the Semidi segment (von Huene et al., 1987;
834 von Huene et al., 2012). Pre- existing structural heterogeneity on the incoming plate can permit
835 fluids to enter the subduction zone and increase the pore pressure, thereby reducing the
836 effective normal stress and making it easier for earthquake rupture to propagate through this
837 region, once initiated. This mechanism is inferred to be responsible for the greater number of
838 intermediate depth earthquakes for the Shumagin and Kodiak segments (Shillington et al.,
839 2015). Our results agree with this interpretation for the southwest Kodiak segment, especially
840 since offset magnetic lineations in the oceanic crust (corresponding to fracture zones), when

841 subducted at the trench, could contribute to fault-bending and be favorable to fluid permeation
842 (Figure 7b).
843
844 ***Kodiak/Kenai segment boundary***
845 The northeastern boundary of the Kodiak segment has been inferred to exist somewhere
846 between the northern Kodiak Islands and the Kenai Peninsula (e.g., von Huene et al., 2012).
847 Although Johnson et al (1996) and Ichinose et al (2007) show an isolated 1964 slip patch
848 between the PWS and Kodiak segments, only recently have geologic observations been made
849 that suggest an independent Kenai segment (e.g.,Hutchinson and Crowell, 2007; Shennan et al.,
850 2014; Kelsey et al., 2015). If so, then it seems likely that there is some structural expression of
851 the segment boundary between the Kodiak Islands and the Kenai Peninsula.
852
853 The 58° fracture zone has been characterized with magnetic and gravity data (Figures 7 and 8).
854 A prominent structural high on the upper plate lies immediately above the subducted 58°
855 fracture zone on the Kodiak forearc and sources the positive gravity lineament on the landward
856 side of the continental shelf break (Figure 7; Fisher, 1980). The trend of both the related
857 anticline and this fracture zone bound the negative gravity anomaly to the north of Kodiak
858 Island (Figure 7a and 8). However, the uplift is Miocene to Pliocene in age (von Huene et al.,
859 1987) and is most likely not associated with subduction of the 58° fracture zone as the depth to
860 the plate interface is nearly 20 to 25 km below the anticline (Hayes et al., 2018). Northwest of
861 the 58° fracture zone trend, however, KSfz scarp heights diminish and offset reflectors in MMS

reflection profiles do not extend to the seafloor. KSfz scarps are not apparent onto the Kenai segment, which suggests the zone of focused uplift (i.e., active splay faulting) does not persist onto the negative gravity anomaly region (Figure 7a). Unfortunately, geodetic inversions lack resolution across the Kodiak/Kenai segment transition, as it lies sufficiently far offshore (Zweck et al., 2002; Freymueller et al., 2008; Li et al., 2016). The Ichinose et al. (2007) slip model shows that the middle asperity is confined to the Kenai Peninsula region and the 58° fracture zone forms a possible southern boundary (Figure 7c); though the influence of a subducted fracture zone is speculative. Thus, there is a structural (KSfz), geophysical (gravity, magnetics), and coseismic expression (slip model) of physical property changes that can be related to inferred plate interface conditions.

The Kodiak and Kenai segment boundary may also be driven by differences in subducting sediment volume. Between the 58° fracture zone and PWS, there is an absence of significant structural relief on the incoming plate and sediment from the Surveyor Fan is the primary material above the oceanic crust (Reece et al., 2011). Seismic reflection profiles show more than one km of sediment near the trench (Fruehn et al., 1999). Assuming enough of the Surveyor Fan has been subducted, this sediment may contribute to the low velocity anomaly, negative free-air gravity, and general lack of thrust earthquakes occurring near the interface below the Kenai Peninsula (Ye et al., 1997; Doser et al., 2002). Furthermore, geomechanical models of forearc basin growth and wedge dynamics show that if sedimentation on the upper

882 plate continues beyond the trench axis, then pervasive internal deformation (i.e., faulting) in
883 the forearc basin is not favored (Fuller et al., 2006).
884
885 Porto and Fitzenz (2016) adopt a Bayesian approach which utilizes earthquake catalog data to
886 assess segment boundaries for the Alaska subduction zone. Their methodology suggests a
887 potential segment boundary northeast of the Kodiak Islands. This is broadly consistent with the
888 along-strike change in focal mechanism character (i.e Figure 7d) and where we interpret the
889 northeast termination of the KSfz.
890
891 **FAULT SEGMENT SUMMARY**
892 We infer from legacy seismic reflection data (MMS profiles) that the KSfz faults are splay faults
893 that diverge from, or near, the megathrust at approximately 30 km depth. This depth is greater
894 than the 20 km depth of the plate interface beneath splay faults in the PWS region (Brocher et
895 al., 1994; Liberty et al., 2013; Haeussler et al., 2015), however, this is likely due to simple Pacific
896 plate subduction below the Kodiak region compared to the additional Yakutat terrane
897 subduction near PWS (Moore et al., 1991; Ye et al., 1997). Focused uplift along the KSfz near
898 the Kodiak Islands shoreline exceeds that of the ABfz in the along-dip direction of the
899 megathrust, and is limited in the along-strike direction by the region of underthrusting to the
900 southwest and subduction of the 58° fracture zone to the northeast. Wells et al. (2003) inferred
901 that crustal duplexing might be the source of the unique gravity signal across the Kodiak
902 Islands. Previous studies near PWS find that splay faulting is assisted by crustal duplexing above

the megathrust (i.e., Liberty et al., 2013 and 2019; Haeussler et al., 2015). Megathrust duplexing is one hypothesis supporting the observed Kodiak Islands gravity character and uplift patterns of the KSfz. We do not have complementary constraints on megathrust geometry at depths greater than 10 km across the central Kodiak Islands, but the Slab2.0 model (Hayes et al., 2018) would place the region of duplexing near 25 km depth to the plate interface.

CONCLUSIONS

We identify and characterize upper plate splay fault uplift patterns that may be driven by plate interface conditions. The active faults that we identify have persisted across the Kodiak Islands offshore region during many Holocene megathrust earthquakes. Subduction of fracture zones, seamounts, and sediments may drive megathrust segmentation and delimit where active splay faults are found along the Gulf of Alaska margin.

A near-shore tsunami risk is present for coastal populations on mainland Kodiak Island. Our tsunami modelling offers an updated view on how tsunamigenic faults uplift in response to megathrust slip offshore of the Kodiak Islands. We find that a short region of the Kodiak Shelf fault zone is consistent with the tsunami source during the GAE because a majority of back-propagated wave fronts converge to one location where we image tall fault scarps (>20 m). We term this tsunamigenic fault the Ugak fault. This fault, and parallel faults of the KSfz should be included in seismic and tsunami hazard analysis of the region.

924 Overall, the spatial variability in the KSfz seafloor scarp height indicates discrete, short (< 30
925 km) uplift patterns, and thus fault segmentation. More detailed, high-resolution bathymetric
926 and seismic reflection data would help to further constrain fault characteristics and slip-rates,
927 especially near proposed segment boundaries.
928

929 **DATA AND RESOURCES**

930 For our tsunami source and fault mapping analysis, we utilize a regional bathymetry dataset to
931 identify Kodiak shelf seafloor scarps (National Geophysical Data Center, 2009. Southern Alaska
932 Coastal Relief Model. National Geophysical Data Center, NOAA. doi:10.7289/V58G8HMQ).
933 Seafloor topographic data is available from NOAA at
934 https://www.ngdc.noaa.gov/mgg/bathymetry/hydro.html. The legacy seismic profiles were
935 obtained as digital scans of stacked travel time images from MMS permit 75-02
936 (https://www.boem.gov/Geological-and-Geophysical-Data-Acquisition-and-Analysis/; Liberty,
937 2013). EMAG2: Earth Magnetic Anomaly Grid (Stefan Maus, 2009) was obtained at the National
938 Geophysical Data Center, NOAA. Model. doi:10.7289/V5MW2F2P. Global marine gravity model
939 from CryoSat-2 and Jason-1 was obtained from the National Geophysical Data Center at
940 https://data.noaa.gov (Sandwell et al., 2014).
941

942 **ACKNOWLEDGEMENTS**

943 We acknowledge the careful, thoughtful reviews of an early version of this study by Drake
944 Singleton. Any use of trade, firm, or product names is for descriptive purposes only and does

945 not imply endorsement by the U.S. Government. Some figures were made with the Generic
946 Mapping Tools (GMT, Wessel and Smith, 1998).

947

REFERENCES

Barcheck, G., G. Abers, A. N. Adams, A. Becel, J. Collins, J. B. Gaherty, P. J. Haeussler, Z. Li, G. Moore, E. Onyango, E. Roland, et al. (2020). The Alaska Amphibious Community Seismic Experiment, *Seismol. Res. Lett.* doi: 10.1785/0220200189.

Bassett, D., and A. B. Watts (2015), Gravity anomalies, crustal structure, and seismicity at subduction zones: 1. Seafloor roughness and subducting relief, *Geochem. Geophys. Geosyst*., 16, 1508–1540, doi:10.1002/ 2014GC005684.

Bécel, A., Shillington, D. J., Delescluse, M., Nedimović, M. R., Abers, G. A., Saffer, D. M., … Kuehn, H. (2017). Tsunamigenic structures in a creeping section of the Alaska subduction zone. *Nature Geoscience*, *10*(8), 609–613. https://doi.org/10.1038/NGEO2990

Blakely, R. J. (1996). Potential theory in gravity and magnetic applications. Cambridge university press.

Briggs, R.W., S. E. Engelhart, A. R. Nelson, T. Dura, A.C. Kemp, P. J. Haeussler, D. R. Corbett, S. J. Angster, and L.-A. Bradley (2014). Uplift and subsidence reveal a nonpersistent megathrust rupture boundary (Sitkinak Island, Alaska), *Geophys. Res. Lett.* 41, 2289–2296.

Brocher, T. M., G. S. Fuis, M. A. Fisher, G. Plafker, M. J. Moses, J. J. Taber, and N. I. Christensen (1994). Mapping the megathrust beneath the northern Gulf of Alaska using wide-angle seismic data*, J. Geophys. Res*. 99, 11,663–11,686.

Bradley, D., Kusky, T., Haeussler, P., Goldfarb, R., Miller, M., Dumoulin, J., Nelson, S.W., Karl, S. (2003). Geologic signature of an early Tertiary ridge subduction in Alaska. In: Sisson, V. B.,

Roeske, S. M., Pavlis, T. L. (Eds.), Geology of the Transpressional Oregon Developed During – Trench Interaction Along the North Pacific Margin, 19-49, *Geol. Soc. Am. Spec. Pap. 371.*

Bruns, T.R. (1983). Model for the origin of the Yakutat block, an accreting terrane in the northern Gulf of Alaska, *Geology*, 11 (12), 718–721.

Carlson, P.R. and Molnia, B.F., (1975). Preliminary isopach map of Holocene sediments, northern Gulf of Alaska. Scale 1:500,000: *U.S. Geol. Surv., Open-File Rep*., 75-507, 1 map sheet.

Carver, G., and G. Plafker (2008). Paleoseismicity and neotectonics of the Aleutian Subduction Zone—An overview, in Activ*e Tectonics and Seismic Potential of Alaska, Geophys. Monogr. Ser. 179*, edited by J. T. Freymueller et al., pp. 43–63, AGU, Washington, D. C., doi:10.1029/179GM03.

Carver, G., Sauber, J., Lettis, W., Witter, R. and Whitney, B. (2008). Active faults on northeastern Kodiak island, Alaska. *Geophysical Monograph Series*, *179*(December 2015), 167–184. https://doi.org/10.1029/179GM09

Cohen, S. C., and J. T. Freymueller (2004). Crustal deformation in the south central Alaska subduction zone, *Adv. Geophys.,* 47, 1–63.

Crameri, F. (2018). Scientific colour-maps. Zenodo. http://doi.org/10.5281/zenodo.1243862

Doser, D., Brown, W. A., and Velasquez, M. (2002), Seismicity of the Kodiak Island region (1964-2001) and its relation to the 1964 Great Alaska Earthquake, *Bull. Seismol. Soc. Am.*, 92, 3269-3292.

988 Doser, D. (2005), Historical Seismicity (1918-1964) of the Kodiak Island Region, *Bull. Seismol.*
989 *Soc. Am.* 95, no. 3, 878-895, doi: 10.1785/0120040175.
990 Eberhart-Phillips, D., D. H. Christensen, T. M. Brocher, R. Hansen, N. A. Ruppert, P. J. Haeussler,
991 and G. A. Abers (2006). Imaging the transition from Aleutian subduction to Yakutat collision
992 in central Alaska, with local earthquakes and active source data, *J. Geophys. Res*. 111,
993 B11303, doi:10.1029/2005JB004240.
994 Finn, S. P., L.M. Liberty, P.J. Haeusslerand T.L. Pratt (2015). Landslides and megathrust splay
995 faults captured by the late Holocene sediment record of eastern Prince William Sound,
996 Alaska. *Bull. Seismol. Soc. Am. 105, no.* 5, 2343–2353. https://doi.org/10.1785/0120140273
997 Fisher, M. A. (1980). Petroleum geology of Kodiak shelf, Alaska. *AAPG Bull.*, **64**, no. 8, 1140-
998 1157.
999 Fisher, M. A., and von Huene, R. (1980). Structure of the upper Cenozoic strata beneath Kodiak
1000 shelf, Alaska*, AAPG Bull*. 64, 1014–1033.
1001 Fruehn, J., von Huene, R., and Fisher, M. (1999), Accretion in the wake of terrane collision: The
1002 Neogene accretionary wedge off Kenai Peninsula, Alaska, *Tectonics*, 18, 263-277.
1003 Fuller, C. W., S.D. Willett, and M.T. Brandon (2006). Formation of forearc basins and their
1004 influence on subduction zone earthquakes. *Geology*, 34, no. 2, 65-68.
1005 Gulick, S. P. S., Jaeger, J. M., Mix, A. C., Asahi, H., Bahlburg, H.,Belanger, C. L.,...Swartz, J. M.
1006 (2015). Mid-Pleistocene climate transition drives net mass loss from rapidly uplifting St.
1007 Elias Mountains, Alaska. *Proceedings of the National Academy of Sciences* 112, 15042–
1008 15047. https://doi.org/10.1073/pnas.1512549112.

1009 Gutscher, M. A., N. Kukowski, J. Malavieille and S. Lallemand, (1998). Episodic imbricate
1010 thrusting and underthrusting: Analog experiments and mechanical analysis applied to the
1011 Alaskan accretionary wedge. *J. Geophys. Res*. 103, no. B5, 10161-10176.
1012 Haeussler, P. J., Armstrong, P. A., Liberty, L. M., Ferguson, K. M., Finn, S. P., Arkle, J. C., and
1013 Pratt, T. L. (2015) Focused exhumation along megathrust splay faults in Prince William
1014 Sound, Alaska, *Quat. Sci. Rev.* 113, 8-22.
1015 Hayes, G., 2018, Slab2 - A Comprehensive Subduction Zone Geometry Model: U.S. Geological
1016 Survey data release, https://doi.org/10.5066/F7PV6JNV.
1017 Hutchinson, I. and Crowell, A. (2007). Recurrence and extent of great earthquakes in southern
1018 alaska during the late Holocene from an analysis of the radiocarbon record of land-level
1019 change and village abandonment, *Radiocarbon*, 49, 3, 1323-1385.
1020 Johnson, J. M., Satake, K., Holdahl, S. R., and Sauber, J. (1996). The 1964 Prince William Sound
1021 earthquake: joint inversion of tsunami and geodetic data, *J. Geophys. Res.*, 101(B1), 523-
1022 532.
1023 Kachadoorian, R. and Plafker, G., 1967, Effects of the earthquake of March 27, 1964 on the
1024 communities of Kodiak and nearby islands: U.S. Geological Survey Professional Paper 542-F,
1025 p. F1-F41.
1026 Kaufman, D. S., and W. F. Manley (2004). Pleistocene maximum and Late Wisconsin glacier
1027 extents across Alaska, U.S.A., in *Quaternary Glaciations—Extent and Chronology, Part II:*
1028 *North America. Developments in Quaternary Science*, vol. 2, edited by J. Ehlers, and P. L.
1029 Gibbard, pp. 9–27, Elsevier, Amsterdam.

Kaufman, D.S.; Young, N.E.; Briner, J.P.; Manley, W.F (2011). Alaska palaeo-glacier atlas (version 2), *Dev. Quat. Sci.*, 15, 427-445. https://doi.org/10.1016/B978-0-444-53447-7.00033-7

Kelsey, H.M., R.C. Witter, S.E. Engelhart, R. Briggs, A., Nelson, P. Haeussler, and D.R. Corbett (2015). Beach ridges as paleoseismic indicators of abrupt coast subsidence during subduction zone earthquakes, and implications for Alaska-Aleutian subduction zone paleoseismology, southeast coast of the Kenai Peninsula, Alaska, *Quat. Science Rev.*, 113, 147-158.

Kim, Y., G. A. Abers, J. Li, D. Christensen, J. Calkins, and S. Rondenay (2014), Alaska Megathrust 2: Imaging the megathrust zone and Yakutat/Pacific plate interface in the Alaska subduction zone, *J. Geophys. Res*. 119, 1924–1941, doi:10.1002/2013JB010581

Ichinose, G., P. Somerville, H. K. Thio, R. Graves, and D. O'Connell (2007), Rupture process of the 1964 Prince William Sound, Alaska, earthquake from the combined inversion of seismic, tsunami, and geodetic data, *J. Geophys. Res*., 112, doi:10.1029/2006JB004728.

Lamb, H. (1932) Hydrodynamics. 6th Edition, Cambridge University Press, Cambridge, 1-8

Lebrun, J. F., Karner, G. D., and Collot, J. Y. (1998), Fracture zone subduction and reactivation across the Puysegur ridge/trench system, southern New Zealand, *J. Geophys. Res.*, 103, 7293-7313.

Li, J., G. A. Abers, Y. H. Kim, and D. Christensen (2013), Alaska megathrust 1: Seismicity 43 years after the great 1964 Alaska megathrust earthquake, *J. Geophys. Res.: Solid Earth*, 118, 4861–4871, doi:10.1002/jgrb.50358.

Li, J., Shillington, D. J., Saffer, D. M., Bécel, A., Nedimović, M. R., Kuehn, H., … Abers, G. A. (2018). Connections between subducted sediment, pore-fluid pressure, and earthquake behavior along the Alaska megathrust. *Geology*, *46*(4), 299–302. https://doi.org/10.1130/G39557.1

Li, S., J. Freymueller, and R. McCaffrey (2016), Slow slip events and time-dependent variations in locking beneath Lower Cook Inlet of the Alaska-Aleutian subduction zone, J. Geophys. Res. Solid Earth, 121, doi:10.1002/2015JB012491.

Liberty, L.M. (2013). Retrieval, Processing, Interpretation and Cataloging of Legacy Seismic Reflection Data, Gulf of Alaska, US Geological Survey Final Technical Report G12AP20078, 17 p., https://earthquake.usgs.gov/cfusion/external_grants/reports/G12AP20078.pdf

Liberty, L.M. (2015). Near Surface Expression of Megathrust Splay Faults, Western Gulf of Alaska, US Geological Survey Final Technical Report #G13AP00021, 17 p, https://earthquake.usgs.gov/cfusion/external_grants/reports/G13AP00021.pdf

Liberty, L.M. and Ramos, M. (2016). Co-seismic rupture patterns over multiple earthquake cycles near Kodiak Island: a collaborative project with USGS personnel, US Geological Survey Final Technical Report #G13AP00021, 17 p, https://earthquake.usgs.gov/cfusion/external_grants/reports/G15AP00042.pdf

Liberty, L. M., Finn, S. P., Haeussler, P. J., Pratt, T. L., and Peterson, A. (2013), Megathrust splay faults at the focus of the Prince William Sound asperity, Alaska, *J. Geophys. Res. 118, no.* 10, 5428–5441. http://doi.org/10.1002/jgrb.50372.

1070 Liberty, L. M., D.S. Brothers, and P.J. Haeussler (2019). Tsunamigenic splay faults imply a long-
1071 term asperity in southern Prince William Sound, Alaska. *Geophys. Res. Lett. 46, 3764–*
1072 *3772*. https://doi.org/10.1029/2018GL081528
1073 Maus, S. (2009). EMAG2: Earth Magnetic Anomaly Grid (2-arc-minute resolution). National
1074 Geophysical Data Center, NOAA. Model. doi:10.7289/V5MW2F2P [May 2016].
1075 Nishenko, S. P. and K.H. Jacob (1990). Seismic potential of the Queen Charlotte-Alaska-Aleutian
1076 seismic zone. *J. Geophys. Res*. ***95****, no.* B3, 2511–2532,
1077 https://doi.org/10.1029/JB095iB03p02511
1078 Moore, J. C., Bryne, T., Plumely, P. W., Reid, M., Gibbons, H., and Coe, R. S. (1983), Paleogene
1079 evolution of the Kodiak Islands, Alaska: Consequences of ridge-trench interaction in a more
1080 southerly latitude, *Tectonics,* 2, 265-293.
1081 Moore, J. C., et al. (1991), EDGE deep seismic reflection transect of the eastern Aleutian arc-
1082 trench layered lower crust reveals underplating and continental growth, *Geology*, 19, 420-
1083 424.
1084 Mankhemthong, N., Doser, D. I., & Pavlis, T. L. (2013). Interpretation of gravity and magnetic
1085 data and development of two-dimensional cross-sectional models for the border ranges
1086 fault system, south-central alaska. *Geosphere*, *9*(2), 242–259.
1087 https://doi.org/10.1130/GES00833.1
1088 Menard, H. W. and T. Atwater (1969). Origin of fracture zone topography. *Nature*, 222(5198),
1089 1037-1040.

1090 Meyer, B, Saltus, R., and Chulliat, A.(2017). EMAG2v3: Earth Magnetic Anomaly Grid (2-arc-
1091 minute resolution). Version 3. NOAA National Centers for Environmental Information.
1092 https://doi.org/10.7289/V5H70CVX. Accessed July 2, 2021.
1093 Naugler, F. P. and Wageman, J. M. (1973), Gulf of Alaska: Magnetic Anomalies, Fracture Zones,
1094 and Plate Interaction, *GSSA Bull.*, 84, 1575-1584.
1095 Nishenko, S.P. and Jacob, K.H., 1990. Seismic potential of the Queen Charlotte-Alaska-Aleutian
1096 seismic zone. *Journal of Geophysical Research: Solid Earth*, *95*(B3), pp.2511-2532.
1097 NOAA National Centers for Environmental Information. 2004: Multibeam Bathymetry Database
1098 (MBBDB). NOAA National Centers for Environmental Information.
1099 https://doi.org/doi:10.7289/V56T0JNC. Accessed [date].
1100 Plafker, G. (1969). Tectonics of the March 27, 1964 Alaska earthquake, *U.S. Geol. Surv. Prof*.
1101 Pap., 543-I, 74 pp.
1102 Plafker, George, and Berg, H.C., eds., 1994, The Geology of Alaska: Geological Society of
1103 America, 1068 p.
1104 Porto, N. M. and D.D. Fitzenz (2016). An alternative segmentation model for the Alaskan
1105 Aleutian megathrust. *Bull. Seismol. Soc. Am. 106, no.* 3, 1125–1132.
1106 https://doi.org/10.1785/0120150235
1107 Reece, R.S., Gulick, S.P.S., Horton, B.K., Christeson, G.L., and Worthington, L.L. (2011), Tectonic
1108 and climatic influence on the evolution of the Surveyor fan and channel system, Gulf of
1109 Alaska, *Geosphere*, 7, 4, 830–844, doi: 10.1130/GES00654.1.

1110 Robinson, D. P. and Watts, A. B. (2006), Earthquake rupture stalled by a subducting fracture
1111 zone, *Science*, 312, 1203-1205.
1112 Ryan, H.F., von Huene, R., Wells, R.E., Scholl, D.W., Kirby, S., and Draut, A.E., (2011). History of
1113 earthquakes and tsunamis along the eastern Aleutian-Alaska megathrust, with implications
1114 for tsunami hazards in the California continental borderland: U.S. Geological Survey
1115 Professional Paper 1795-A, 31 p.
1116 Sandwell, D. T. (1984), Thermomechanical evolution of oceanic fracture zones, *J. Geophys. Res.,*
1117 89 (B13), 11401-1113
1118 Sandwell, D. T., R. D. Müller, W. H. F. Smith, E. Garcia, R. Francis (2014), New global marine
1119 gravity model from CryoSat-2 and Jason-1 reveals buried tectonic structure, *Science*, 346
1120 (6205), 65-67, doi: 10.1126/science.1258213.
1121 Saltus, R. W., T. L. Hudson, and F. H. Wilson (2007). The geophysical character of southern
1122 Alaska—Implications for crustal evolution, in Tectonic Growth of a Collisional Continental
1123 Margin: Crustal Evolution of Southern Alaska, USA, K. D. Ridgway, J. M. Trop, J. M. G. Glen,
1124 and J. M. O'Neill (Editors), Geol. Soc. Am. Spec. Pap. 431, Boulder, Colorado, 1–20.
1125 Sauber, J., G. Carver, S. Cohen, and R. King (2006), Crustal deformation and the seismic cycle
1126 across the Kodiak Islands, Alaska, *J. Geophys. Res*., 111, B02403,
1127 doi:10.1029/2005JB003626.
1128 Shennan, I., N. Barlow, G. Carver, F. Davies, E. Garrett, and E. Hocking (2014). Great
1129 tsunamigenic earthquakes during the past 1000 yr on the Alaska megathrust, *Geology*, 42,
1130 687-690.

1131 Shennan, I., Brader, M. D., Barlow, N. L. M., Davies, F. P., Longley, C., & Tunstall, N. (2018). Late
1132 Holocene paleoseismology of Shuyak Island, Alaska, *Quat. Sci. Rev. 201*, 380–395.
1133 https://doi.org/10.1016/j.quascirev.2018.10.028
1134 Shillington, D.J.; Bécel, A., Nedimović, M.R., Kuehn, H., Webb, S.C. Abers, G.A., Keranen, K.M.;
1135 Li, J.; Delecluse, M.; Mattei-Salicrup, G.A. (2015), Link between plate fabric, hydration and
1136 subduction zone seismicity in Alaska, *Nature Geosci.*, 8, 961-964, doi:10.1038/ngeo02586
1137 Smith, W. H. F. and Sandwell, D. T. (1997), Global seafloor topography from satellite altimetry
1138 and ship depth soundings, *Science*, 277, 1957-1962.
1139 Song, T. A. and Simons, M. (2003) Large trench-parallel gravity variations predict seismogenic
1140 behavior in subduction zones, *Science*, 301, 630-632.
1141 Suleimani, E., and J. T. Freymueller (2020). Near-field modeling of the 1964 Alaska tsunami: The
1142 role of splay faults and horizontal displacements, *J. Geophys. Res. Solid Earth* **125**, 1–23,
1143 doi: 10.1029/ 2020JB019620.
1144 Suito, H., and J. T. Freymueller (2009). A viscoelastic and afterslip postseismic deformation
1145 model for the 1964 Alaska earthquake, *J. Geophys. Res **114**,* doi:10.1029/ 2008JB005954.
1146 von Huene, R., M. Hampton, M. Fisher, D. Varchol, and G. Cochrane (1980). Map showing near-
1147 surface geologic structures of Kodiak Shelf, Alaska, *U.S. Geol. Surv. Miscellaneous Field*
1148 *Studies Map MF-1200*, 1 sheet, 1:500,000 scale.
1149 von Huene, R., Fisher, M. A., and Bruns, T. R. (1987). Geology and evolution of the Kodiak
1150 margin, Gulf of Alaska, in Geology and Resource Potential of the Continental Margin of
1151 Western North America and Adjacent Ocean Basins-Beaufort Sea to Baja California, Scholl,

D. W., Grantz, A., and Vedder, J. G., (eds.): Houston, Texas, Circum-Pacific Council for Energy and Mineral Resources, p. 191-212.

von Huene, R., Klaeschen, D., and Fruehn, J. (1999). Relation between the Subducting Plate and Seismicity Associated with the Great 1964 Alaska Earthquake, *Pure and App. Geophys.*, 154, 575-591.

von Huene, R., J. J. Miller, and W. Weinrebe (2012). Subducting plate geology in three great earthquake ruptures of the western Alaska margin, Kodiak to Unimak, *Geosphere*, 8(3), 628–644.

Wang, K., and Hu, Y. (2006). Accretionary prisms in subduction earthquake cycles: The theory of dynamic Coulomb wedge, *J. Geophys. Res.*, 111, B06410, doi:10.1029/2005JB004094.

Wang, K. and S. Bilek (2011). Do subducting seamounts generate or stop large earthquakes? *Geology,* 39, 819-822.

Wells, D. L., & Coppersmith, K. J. (1994). New Empirical Relationships among Magnitude, Rupture Length, Rupture Width, Rupture Area, and Surface Displacement. *Bull. Seismol. Soc. Am. 84, no.* 4, 974–1002.

Wells, R. E., R. J. Blakely, Y. Sugiyama, D. W. Scholl, and P. A. Dinterman (2003). Basin-centered asperities in great subduction zone earthquakes: A link between slip, subsidence, and subduction erosion?, *J. Geophys. Res*., 108(B10), 2507, doi:10.1029/2002JB002072.

Ye, S., Flueh, E. R., Klaeschen, D., and von Huene, R. (1997). Crustal structure along the EDGE transect beneath the Kodiak shelf off Alaska derived from OBH seismic refraction data, *Geophys. J. Int.*, 130, 283-302.

1173 Zimmermann, M., Prescott, M.M. and Haeussler, P.J., 2019. Bathymetry and geomorphology of
1174 Shelikof Strait and the Western Gulf of Alaska. *Geosciences*, *9*(10), p.409.
1175 Zweck, C., Freymueller, J. T., and Cohen, S. C. (2002). Three-dimensional elastic dislocation
1176 modeling of the postseismic response to the 1964 Alaska earthquake, *J. Geophys. Res.*, 107,
1177 10.1029/2001.
1178